the protein disulfide isomerase family, involved in protein maturation and folding, on the basis of structural similarity.[9] Several studies have shown that AGR2 is overexpressed and promoted tumor progression in numerous human malignancies affecting the ovary, breast, lung, prostate, and pancreas.[10–14]

In PDAC, Ramanchandran *et al.*[14] reported that AGR2 expression was elevated, even in PanIN1A, the earliest precursor lesion of PDAC. In this context, AGR2 promotes cancer cell proliferation, invasion, and resistance to chemotherapy, suggesting that AGR2 promotes cancer progression; however, the mechanisms underlying AGR2 function in advanced PDAC remain unclear. The prognostic value of AGR2 expression in PDAC is controversial.[15] Previous reports have also shown that AGR2 promotes dissemination of pancreatic cancer via regulation of lysosomal proteases (cathepsin B and D); however, conversely, AGR2 expression is decreased in PDAC compared with PanIN.[16]

Epithelial–mesenchymal transition (EMT), a well-known hallmark of highly invasive cancer cells, is a critical phenotypic alteration involved in the morphological change from epithelial to mesenchymal phenotype. Emerging evidence suggests that the acquisition of a mesenchymal phenotype has a key role in migration, invasion, resistance to chemoradiotherapy, and extravasation of cancer cells from the primary tumor microenvironment.[17] Other studies have revealed that decreased membranous expression and cytoplasmic translocation of E-cadherin provide an indication of EMT.[18,19] Furthermore, EMT is correlated with high histological grade in breast and pancreatic cancer.[20] To the best of our knowledge, however, there are no studies addressing the correlation between AGR2 expression and EMT induction.

The tumor microenvironment, which is composed of immune cells, fibroblastic cells, blood vessels, and extracellular matrix in cancer stroma, closely interacts with cancer cells invading the stroma. Pancreatic stellate cells (PSCs), having myofibroblastic morphology in activated state, are located in the pancreatic stroma and have an important role in the pancreatic cancer microenvironment.[21] The interaction between pancreatic cancer cells and PSCs promotes cancer cell proliferation, migration, and invasion via the secretion of soluble factors, such as transforming growth factor beta-1 (TGF-β1), epidermal growth factor (EGF), and fibroblast growth factor 2 (FGF-2), which are well-characterized EMT-inducible factors.[22–26] A recent report demonstrated that PSCs also promote EMT in pancreatic cancer cells.[27]

In this study, we aim to verify whether AGR2 expression represents a useful prognostic marker in human PDAC, and whether its downregulation is mediated by EMT induction. We identified a correlation between AGR2 expression, EMT marker expression, and clinic-pathological parameters in PDAC. Our study also shows that preserved AGR2 expression is a favorable prognostic factor in PDAC.

MATERIALS AND METHODS

Patients and Tissue Samples

Formalin-fixed, paraffin-embedded surgical resection samples (PDAC, $n=195$, PanIN, $n=15$, and IPMN, $n=39$) were obtained from patients who were diagnosed and underwent pancreatic resection at our institution between July 1999 and March 2009. Forty variants of pancreatic cancer including adenosquamous carcinoma ($n=4$), adenocarcinoma with squamous differentiation ($n=6$), anaplastic carcinoma ($n=3$), and acinar cell carcinoma ($n=1$) were excluded from this study. The study protocol was approved by the Ethics Committee of Kyushu University (approval number 24–222, 25–117) and conformed to the Ethical Guidelines for Human Genome/Gene Research enacted by the Japanese Government and the Declaration of Helsinki. For strict privacy protection, identifying information for all patients was removed before analysis.

Immunohistochemical Analysis

Primary antibodies used for immunohistochemical (IHC) analysis were as follows: AGR2 (rabbit polyclonal, IMG-5279A, 1/100 dilution, IMGENEX, San Diego, CA, USA), vimentin (mouse monoclonal, Clone V9, 1/25 dilution, DAKO Cytomation, Glostrup, Denmark) and E-cadherin (mouse monoclonal, 610181, 1/1000 dilution, BD Biosciences, Franklin Lakes, NJ, USA). Antibodies were diluted in 5% dry skimmed milk in PBS. In brief, 5-μm-thick tissue sections were deparaffinized in xylene and dehydrated in ethanol. Endogenous peroxidase activity was blocked by incubation in methanol containing 0.3% H_2O_2 for 30 min. Antigen retrieval was achieved by boiling slides in a microwave in 10 mM citrate buffer (pH 6.0) for 20 min (AGR2 and E-cadherin only). The slides were then incubated with primary antibodies at 4 °C overnight and subsequently incubated with biotin-free horseradish peroxidase enzyme-labeled polymer (Envision plus System, DAKO Cytomation) for 40 min at room temperature. The labeled antigens were visualized using 3,3′-diaminobenzidine tetrahydrochloride as a chromogen. Counterstaining was performed with hematoxylin. Appropriate positive and negative controls were performed for all antibodies. Nonspecific staining was not observed in any negative-control sections.

Evaluation of Immunohistochemical Staining

All tissue sections were assessed by two investigators (YM and SA) who were blinded to patient clinicopathological results. AGR2 immunoreactivity was determined using an intensity score, graded on a scale from 0 to 3, and a proportional score, corresponding to the percentage of stained cells (0: no staining, 1: < 20%; 2: 20–50%, and 3: > 50%), as previously described.[16] The total score was the product of intensity and the proportional score. AGR2 high-expressing patients scored between 4 and 6 ($n=139$) and low-expressing patients between 0 and 3 ($n=54$). Membranous immunoreactivity for E-cadherin was categorized as high expression (> 50% of

cells staining positive, similar to normal epithelial cells) or low expression (<50% of cells staining positive), as previously described.[28] Cytoplasmic expression of vimentin was categorized as positive if any cancer cell exhibited positive immunoreactivity and as negative if there was complete absence of vimentin staining.

Cells and Culture Conditions

The following pancreatic cancer cell lines were used in this study: HPC-3, H48N (Dr H Iguchi, National Shikoku Cancer Center, Matsuyama, Japan), Panc-1 (Riken Cell Bank, Tsukuba, Japan), SUIT-2, MIA PaCa-2 (Japanese Cancer Resource Bank, Osaka, Japan), HS766T, BxPC-3, Capan-2, Aspc-1, and CFPAC-1 (American Type Culture Collection, Manassas, VA, USA). Human PSCs were isolated from PDAC surgical specimens using the outgrowth method as previously described.[21] Primary cultures of PSCs derived from PDAC patients were established in our laboratory. These cells exhibited a fibroblast-like morphology, and immunofluorescence analysis revealed that the majority of cells were positive for vimentin and alpha-smooth muscle actin (>90%), markers of activated fibroblasts and glial fibrillary acidic protein, a marker of PSCs, and negative for cytokeratin 19, a marker of epithelial cells (Supplementary Figure 1). All established PSCs were used between passages 3 and 7. All cells were maintained in Dulbecco's modified Eagle's medium (DMEM) (Life Technology, Grand Island, NY, USA) supplemented with 10% fetal bovine serum (FBS) (Invitrogen, Carlsbad, CA, USA), streptomycin (100 mg/ml) and penicillin (100 mg/ml) and grown at 37 °C in a humidified atmosphere containing 10% CO_2.

Western Blotting

Protein was extracted from cell lines using lysis buffer (PRO-PREP Protein Extraction Solution, iNtRON Biotechnology, Seongnam, South Korea), and lysates (20 μg) were separated by SDS-PAGE and transferred to polyvinylidene difluoride membranes (Immobilon P, Millipore, Bedford, MA, USA). Membranes were blocked with 5% dry skimmed milk and incubated with primary antibodies; anti-AGR2 rabbit polyclonal antibody (1:500, IMGENEX), anti-E-cadherin mouse polyclonal antibody (1:5000, BD Biosciences), anti-vimentin mouse monoclonal antibody (1:500, DAKO Cytomation), anti-phospho-Smad2 (Ser465/467)/Smad3 (Ser423/425) rabbit monoclonal antibody (#8828, 1:1000, Cell Signaling Technology, Danvers, MA, USA), anti-Smad2/3 rabbit monoclonal antibody (#8685, 1:1000, Cell Signaling Technology), anti-phospho-p44/42 MAPK (Erk1/2) (Thr202/Tyr204) rabbit monoclonal antibody (#4370, 1:2000, Cell Signaling Technology), and anti-p44/42 MAPK (Erk1/2) rabbit monoclonal antibody (#4695, 1:1000, Cell Signaling Technology) using the SNAP i.d. Protein Detection System (Millipore) in accordance with the manufacturer's instructions. Anti-glyceraldehyde 3-phosphate dehydrogenase antibody (mouse monoclonal, sc32233, 1/5000 dilution, Santa Cruz Biotechnology, Santa Cruz, CA, USA) was used as an internal control. Membranes were then incubated with anti-rabbit IgG (#7074, 1/5000 dilution, Cell Signaling Technology), anti-mouse IgG1 (sc-2061, 1/3000 dilution, Santa Cruz Biotechnology), and anti-mouse IgG2a (sc-2061, 1/3000 dilution, Santa Cruz Biotechnology). Immunoreactive signals were detected using ECL Prime (GE Healthcare, Buckinghamshire, UK) and images were acquired using a ChemiDoc XRS (Bio-Rad Laboratories, Hercules, CA, USA).

Quantitative RT-PCR (qRT-PCR)

qRT-PCR was performed as previously described.[29] Total RNA was isolated from cancer cell lines using the High Pure RNA Isolation Kit (Roche Diagnostics, Mannheim, Germany) with DNase I (Roche Diagnostics) treatment, in accordance with the manufacturer's instructions. RNA was quantified by measuring absorbance at 260 nm, and purity was evaluated from the 260/280 ratio of absorbance using a NanoDrop ND-1000 spectrophotometer (NanoDrop Technologies, Wilmington, DE, USA). qRT-PCR was performed using the QuantiTect SYBR Green Reverse Transcription-PCR kit (Qiagen, Tokyo, Japan) and a CFX96 Touch Real-Time PCR Detection System (Bio-Rad Laboratories). Data are presented as relative expression normalized to 18S rRNA levels. The primer sequences are listed in Supplementary Table 1.

Immunofluorescence Staining

Primary-cultured PSCs were seeded in 35-mm glass-bottom dishes (Matsunami, Osaka, Japan) (2×10^4 cells/dish) in DMEM with 10% FBS and incubated for 24 h. Cells were then fixed with methanol, blocked with 3% bovine serum albumin in PBS, and incubated with either anti-alpha-smooth muscle actin antibody (rabbit polyclonal, ab5694, 1/100 dilution, Abcam, Cambridge, MA, USA), anti-vimentin antibody (mouse monoclonal, clone V9, 1/50 dilution, Dako), anti-glial fibrillary acidic protein antibody (mouse monoclonal, ab10062, 1/100 dilution, Abcam), and anti-cytokeratin 19 antibody (goat polyclonal, sc-33111, 1/5000 dilution, Santa Cruz Biotechnology) overnight at 4 °C. Cells were then incubated with Alexa 488-conjugated anti-mouse IgG (A11029, Molecular Probes, Eugene, OR, USA), 546-conjugated anti-rabbit IgG (A11035, Molecular Probes), or 546-conjugated anti-goat IgG (A11056, Molecular Probes) for 1 h. Nuclear DNA was counterstained with 4′,6-diamidino-2-phenylindole (0.05 μg/ml) (Dojindo, Kumamoto, Japan). Fluorescence was visualized using an All-in-one Type Fluorescence Microscope (BZ-9000; Keyence Corporation, Osaka, Japan), and images were acquired using BZ-II image analysis software (Keyence).

AGR2 Knockdown by Small-Interfering RNA (siRNA)

siRNA targeting AGR2 (On-Target plus Smart Pool siRNAs-siAGR2) and non-targeting siRNA control (ON-TARGET plus non-targeting siRNA) were purchased from Dharmacon

(Chicago, IL, USA). Transfection was performed according to the manufacturer's reverse-transfection protocol using Lipofectamine RNAiMAX (Life Technology). In brief, siRNAs and Lipofectamine (5 μl) were diluted in 500 μl Opti-MEM (Life Technology) without serum, and incubated for 10 min at room temperature. Cancer cells (3×10^5) were resuspended in 2.5 ml of DMEM supplemented with 10% FBS without antibiotics. The siRNA and Lipofectamine mixture was added to the diluted cells (3 ml final volume, final siRNA concentration 2 nM for Aspc-1 cells and 10 nM for Panc-1, Hs766T, Capan-2, and BxPC-3 cells) and seeded in six-well plates (3×10^5 cells/well). After 24-h incubation, plates were washed and cells were incubated in complete growth medium (DMEM with 10% FBS and antibiotics) for various time points. Cancer cells were used in subsequent experiments 48 h post transfection.

Proliferation Assays

Cancer cell lines were seeded in 24-well plates (1×10^4 cells/well) (Becton Dickinson, Bedford, MA, USA) in DMEM containing 10% FBS. Following incubation for the indicated times (0, 1, 3, or 5 days), propidium iodide (30 μmol/l) and digitonin (600 μmol/l) were added to each well to label cell nuclei. Cell proliferation was evaluated by measuring the fluorescence intensity of propidium iodide, as previously described[30] using an infinite F200 (Tecan, Männedorf, Switzerland).

Colony Formation Assays

Anchorage-independent growth was assessed by colony formation in soft agar as previously described.[31] Single-cancer cells (1×10^4 cells) were diluted in DMEM with 10% FBS and 0.35% Bacto-Agar (Difco, Detroit, MI, USA), and seeded in six-well plates on top of a 0.7% agar bottom layer without cells. Cells were incubated for 14 days, and growth medium (DMEM with 10% FBS) was replaced biweekly. Colonies were stained with crystal violet (0.005%) for 20 min and counted under a light microscope.

Matrigel Invasion and Migration Assays

Cancer cell migration and invasiveness were assessed by determining the number of cells invading 8-μm pore Transwell chambers (BD Biosciences). Transwell inserts were coated with Matrigel (20 μg/well; BD Biosciences, Bedford, MA, USA) for invasion assays, and without coating for migration assays. For indirect co-culture experiments, PDAC cell lines (4×10^4 cells) were resuspended in 250 μl of DMEM containing 1% FBS, and seeded in the upper chamber, which was then placed in a 24-well culture dish containing PSCs (4×10^4 cells) resuspended in 750 μl of the same medium. For monoculture experiments using AGR2 knockdown cells, cancer cells (4×10^4 cells) were resuspended in 250 μl of DMEM containing 10% FBS and seeded in the upper chamber, which was placed in a 24-well culture dish containing 750 μl of the same medium. Invasion and migrations assays were performed using Aspc-1 and Hs766T cells for 36 and 24 h, respectively. Invading or migrating cancer cells were fixed to the lower surface of the transwell membrane with 70% ethanol, stained with hematoxylin–eosin and counted in five random fields at $\times 100$ magnification, using an All-in-one Type Fluorescence Microscope (BZ-9000; Keyence) and BZ-II image analysis software (Keyence). Results are expressed as the mean number of cancer cells translocating to the lower surface.

Indirect Co-Culture of Cancer Cells with PSCs

Indirect co-culture experiments were performed as previously described.[27] Pancreatic cancer cells (1×10^5 cells) were seeded in six-well plates (BD Biosciences) in 2 ml DMEM supplemented with 10% FBS. Human primary-cultured PSCs (3×10^5 cells) were seeded into 3-μm pore Transwell chambers in 1 ml DMEM with 10% FBS. The following day, Transwell chambers seeded with PSCs were placed into six-well plates containing pancreatic cancer cells, and incubated up to 48 h in DMEM with 1% FBS.

Treatment with Recombinant Proteins

To identify the factors involved in AGR2 downregulation, we cultured cancer cells in the presence of recombinant human TGF-β1, EGF, and FGF-2, which have previously been shown to induce EMT.[24–26] Cancer cells were seeded in 90-mm dishes (1×10^5 cells/dish) and incubated for 48 h in DMEM supplemented with 1% FBS with or without various growth factors (0.5, 1, 2, and 5 ng/ml recombinant human TGF-β1 (R&D Systems, Oxon, UK), 1, 10, and 100 ng/ml recombinant human FGF-2 (Sigma, Basel, Switzerland), and 1, 10, 20, and 100 ng/ml recombinant human EGF (Sigma).

Enzyme-Linked Immunosorbent Assay (ELISA) for TGF-β1 Levels

Secreted TGF-β1 levels were assayed in cell culture supernatants using the Quantikine human TGF-β1 kit (R&D Systems). Aspc-1 cells (1×10^5 cells) were plated in six-well plates and co-cultured with or without primary-cultured PSCs (3×10^5 cells) for 24 h in serum-free DMEM. Supernatants were then collected and analyzed in accordance with the manufacturer's instructions. Cancer cells were co-cultured with PSCs as described above. Each sample was assayed in triplicate and quantification was obtained using a plate reader at 450 nm (corrected by subtracting absorbance at 540 nm).

Inhibition of TGF-β Signaling Using Neutralizing Antibody

For inhibition of TGF-β signaling, PDAC cells were co-cultured with PSCs as described above, and treated with recombinant human TGF-β sRII/Fc (rhTβsR-II) (100 ng/ml, 341-BR, R&D Systems),[32] TGF-β neutralizing antibody (10 μg/ml, MAB1835, R&D Systems) or mouse control IgG1 (10 μg/ml, MAB002,

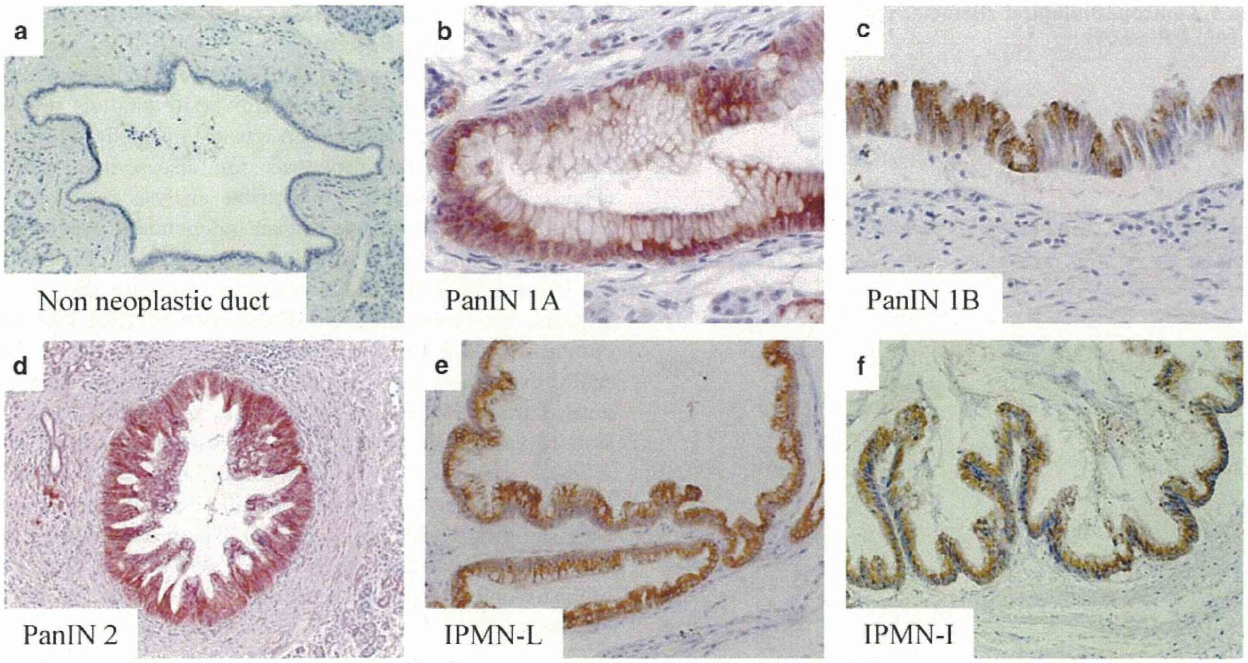

Figure 1 Immunohistochemical analysis of anterior gradient 2 (AGR2) in chronic pancreatitis and pre-cancerous lesions. AGR2 expression was not detected in non-neoplastic ducts of chronic pancreatitis patients (**a**). AGR2 upregulation was observed in benign PDAC precursor lesions including PanIN1A (**b**) and IPMN with low-grade dysplasia (**e**), and expression was retained in more severe precursor lesions (**c**, **d** and **f**). PanIN, pancreatic intraepithelial neoplasia; IPMN-L, intraductal papillary mucinous neoplasm with low-grade dysplasia; IPMN-I, intraductal papillary mucinous neoplasm with intermediate-grade dysplasia; (original magnification: (**a**) ×100, (**b**) ×200, (**c**) ×200, (**d**) ×40, (**e**) ×100, (**f**) ×100).

R&D Systems) for 48 h in DMEM supplemented with 1% FBS.

Statistical Analysis

The correlation between two variables was analyzed using the χ^2-test or the Fisher exact test, where appropriate. For survival analysis, disease-free survival was adopted as primary end points. The survival correlation was presented using Kaplan–Meier analysis, and the curves were compared using the log-rank test. Linear regression analysis was used to examine the association between mRNA levels of AGR2 and E-cadherin in PDAC cell lines. For *in vitro* experiments, continuous variables were expressed as the mean ± s.d. Each experiment was performed in biological triplicate. Comparison between two groups was analyzed using the Student's *t*-test. Statistical significance was defined as $P<0.05$. All statistical analyses were performed using JMP 9.01 software (SAS Institute, Cary, NC, USA).

RESULTS

AGR2 Expression in PDAC and Pre-Cancerous Lesions

IHC analyses revealed AGR2 staining in the cytoplasm of neoplastic cells. All PDAC precursors were positive for AGR2 expression, even in PanIN1A (100%, 10/10) and IPMN with low-grade dysplasia (100%, 20/20), which represent the most benign types of PDAC precursor lesions. AGR2 expression was retained in PanIN2 (100% 5/5) and IPMN with intermediate-grade dysplasia (100%, 19/19). In contrast, AGR2 immunoreactivity was not detected in normal pancreatic duct specimens of chronic pancreatitis patients (Figure 1). Clinicopathological findings and IHC characteristics for AGR2 are summarized in Table 1. Of the 195 PDAC patients, AGR2 expression was decreased in 54 patients (27.7%). Decreased AGR2 expression was associated with high histological grade (G3 (poorly differentiated); refer to structure, growth pattern of the cancer cells, and nuclear atypia) ($P<0.0001$) and high Union for International Cancer Control stage (>stage II) ($P=0.0061$).

Reduced Expression of AGR2 Correlates with Markers of EMT in PDAC

We observed decreased expression of AGR2 in areas of high histological grade and decreased cell adhesiveness in the tissue of PDAC patient (Figures 2a–h). Therefore, we hypothesized that EMT may be associated with AGR2 downregulation. To assess this hypothesis, we investigated the expression of EMT markers (E-cadherin and vimentin) in serial sections of PDACs by IHC staining. In Table 1, membranous E-cadherin expression was reduced (<50%) in 68 patients (34.9%) and cytoplasmic vimentin expression was observed in 36 patients (18.5%), and AGR2 downregulation

Table 1 Clinicopathological characteristics of PDAC patients ($n = 195$) (*$P < 0.01$)

	AGR2 expression		Total	
Variable	High ($n = 141$)	Low ($n = 54$)	($n = 195$)	*P*-value
Age (in years)	66.5 (36–86)	63.7 (36–80)		
Male/female	84/57	37/17	121	0.2494
Location				
Head/body and tail	96/43	33/21	129/63	0.3885
E-cadherin				
High expression	114	13	127	<0.0001*
Low expression	27	41	68	
Vimentin				
Positive	14	22	36	<0.0001*
Negative	127	32	159	
Histological grade				<0.0001*
G1 (well)	42	2		
G2 (moderately)	60	9		
G3 (poorly)	27	38		
Local invasion	118/139 (84.9%)	49/53 (92.3%)		0.164
Vessel invasion	111/141 (78.7%)	46/53 (86.8%)		0.2024
Lymph node metastasis	95/141 (67.4%)	43/54 (79.6%)		0.0923
UICC T category				
1/2	14	5	19	0.8878
3/4	127	49	176	
UICC stage				
Stage I/II	137	47	184	0.0061*
Stage III/IV	4	7	11	

Abbreviations: AGR2, anterior gradient 2; PDAC, pancreatic ductal adenocarcinoma; UICC, Union for International Cancer Control.

was associated with reduced membranous E-cadherin expression ($P < 0.0001$) and cytoplasmic vimentin expression ($P < 0.0001$). Areas of reduced AGR2 expression were consistent with those exhibiting induction of EMT (decreased membranous expression of E-cadherin and positive cytoplasmic vimentin expression) (Figures 2c, d, g, h, k, l, o and p). These data demonstrate that AGR2 downregulation is correlated with induction of EMT, probing a deeper analysis of the interaction between these two parameters.

Reduced Expression of AGR2 Correlates with Poor Prognosis in PDAC Patients

We next examined the relationship between AGR2 expression and survival of PDAC patients. Univariate analysis revealed that decreased AGR2 expression was a statistically significant indicator of adverse prognosis for disease-free survival (Figure 3a). Conversely, multivariate analysis revealed that AGR2 downregulation was not an independent predictor of shorter overall survival (Supplementary Table 2). To examine the impact of AGR2 and E-cadherin status on disease-free survival, we determined the disease-free survival rate with combined AGR2 and E-cadherin status (Figures 3b–d). Low AGR2 expression was correlated with poor disease-free survival. Further evaluation on the basis of E-cadherin expression revealed that lower AGR2 expression correlated with a lower survival rate in both high- and low-E-cadherin expression cohorts, although this difference was not statistically significant (Figures 3c and d). These data suggest that AGR2 downregulation could contribute to poor prognosis, but is partially affected by decreased membranous E-cadherin expression.

AGR2 Expression in Pancreatic Cancer Cell Lines

Analysis of *AGR2* expression in a panel of nine pancreatic cancer cell lines by qRT-PCR revealed significant variation in expression levels. Epithelial-type cancer cell line (high E-cadherin, low vimentin; HS766T, H48N, and BxPC-3) exhibiting cellular adhesiveness retained *AGR2* expression, whereas spindle-shaped mesenchymal-type cancer cell line (low E-cadherin, high vimentin; MiaPaCa2, SUIT-2, and HPC-3) expressed relatively low levels of *AGR2* (Figure 4a). Linear regression analysis revealed a strong positive correlation between AGR2 and E-cadherin expression at the mRNA level (Figure 4b; $R^2 = 0.7262$, $P = 0.0035$). Taken together, these results strengthen the hypothesis that *AGR2* downregulation is correlated with EMT induction.

AGR2 Knockdown Using siRNA

To analyze the function of AGR2 *in vitro*, we performed targeted knockdown of AGR2 in PDAC cells using anti-AGR2 siRNA. Efficient knockdown of *AGR2* transcript (>70% until 120 h post transfection) was confirmed by qRT-PCR (Figures 5a and g), and reduced AGR2 protein levels were confirmed by western blot 72 h post transfection (Figure 5b). Targeted inhibition of AGR2 in both Aspc-1 and Hs766T cells led to a significant decrease in anchorage-dependent cell proliferation (Figure 5c), colony formation (Figure 5d), cell migration (Figure 5e), and cell invasiveness (Figure 5f) compared with cells transfected with non-coding negative-control RNA ($P < 0.05$), except for the colony formation assay in Hs766T ($P = 0.0686$). AGR2 knockdown did not alter the expression of epithelial or mesenchymal markers (E-cadherin and vimentin, respectively), or transcription factors involved in EMT induction (Snail-1, Snail-2, and ZEB-1) in PDAC cells (Figure 5g), implying that AGR2 does

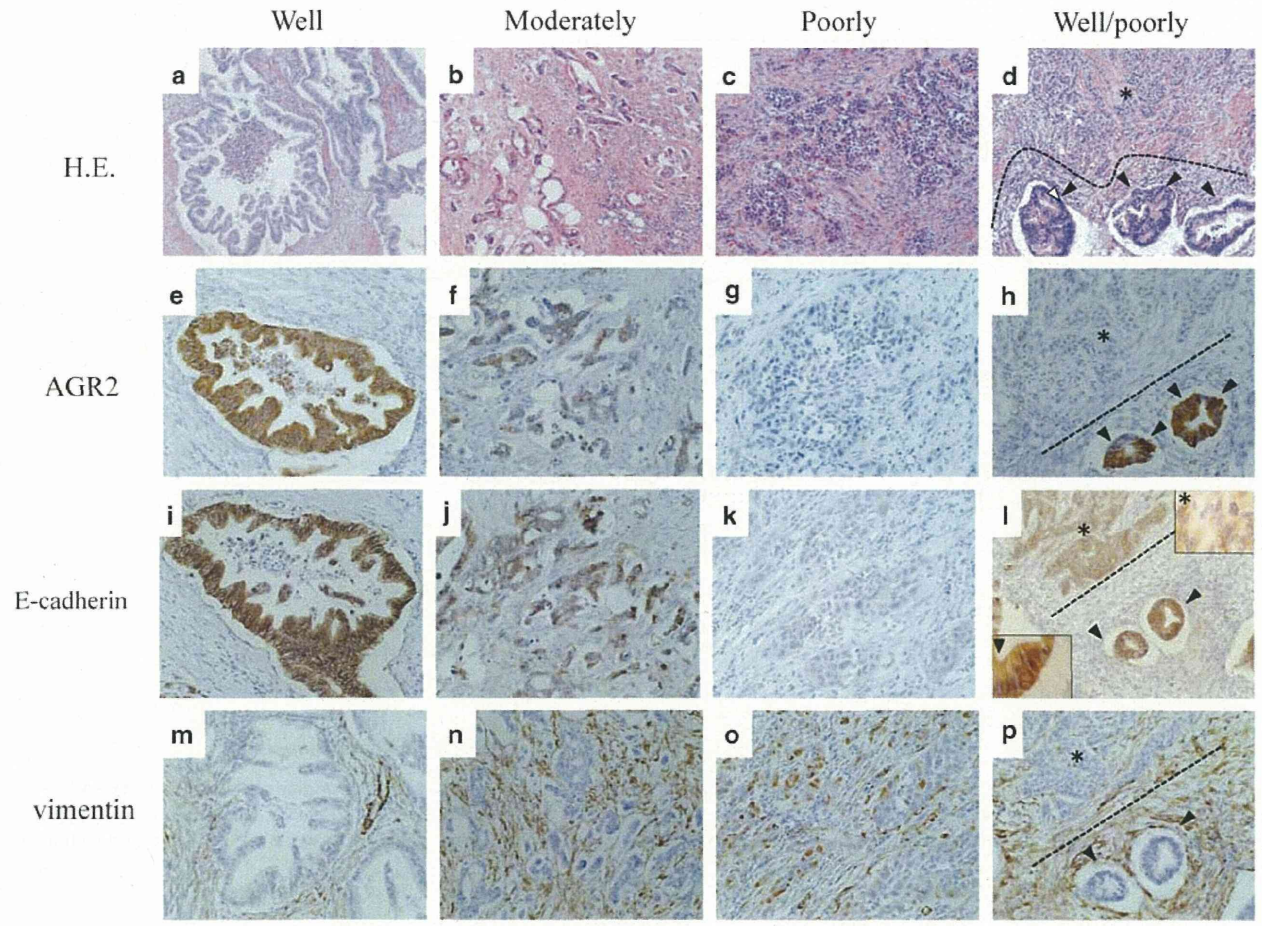

Figure 2 Histological analyses of human PDAC specimens. Representative images of hematoxylin and eosin (H&E) staining (**a–d**) and immunohistochemical staining for anterior gradient 2 (AGR2) (**e–h**), E-cadherin (**i–l**), and vimentin (**m–p**). Each column of figures represent serial sections of one PDAC patient (**a**, **e**, **i** and **m**: well differentiated; **b**, **f**, **j** and **n**: moderately differentiated; **c**, **g**, **k** and **o**: poorly differentiated; **d**, **h**, **l** and **p**: admixed components of well- (arrowhead) and poorly (asterisk) differentiated adenocarcinoma. Low-histological-cellular-grade (well or moderately differentiated) PDAC retained AGR2 and membranous E-cadherin expression, whereas vimentin expression was absent. Cytoplasmic AGR2 expression and membranous E-cadherin expression were decreased in parallel with cancer de-differentiation, and positive cytoplasmic vimentin expression was observed in high-histological-cellular-grade (poorly differentiated) PDAC. E-cadherin expression is seen at the membrane and in the cytoplasm of the well-differentiated carcinoma, but is decreased in the membrane of the poorly differentiated carcinoma (**l**; insets). Original magnification: H&E staining ×100, IHC ×200.

not directly regulate EMT induction in PDAC cells. These results are consistent with previous reports, but not our IHC data. It was suggested that correlation with adverse prognosis and EMT induction in low-AGR2-expressing PDAC patients by our IHC analysis was not due to loss of AGR2 function itself. On the basis of these observations, we hypothesize that other molecules involved in PDAC progression function as upstream negative regulators of AGR2.

AGR2 Expression Decreased in PDAC Cell Lines Co-Cultured with PSCs

Among the mechanisms promoting cancer progression, cancer-stromal interactions have a crucial role in cancer cells invading the tumor microenvironment, but not in intraepithelial lesions. To investigate the relationship between AGR2 downregulation, tumor microenvironment and EMT induction, we performed co-culture experiments, in which PDAC cells were indirectly co-cultured with human primary-cultured PSCs. Co-culture of PDAC cells with primary PSCs induced EMT, as evidenced by a decrease in E-cadherin and increase in vimentin, Snail-1, Snail-2, and ZEB-1 mRNA levels, compared with cancer cell monocultures (Figures 6b and c), and E-cadherin and vimentin expression was slightly altered in protein levels. AGR2 expression was decreased in co-cultured PDAC cells at the mRNA and protein levels (Figures 6a and d). The results of these indirect co-culture experiments suggest that soluble factors secreted from PSCs contribute to AGR2 downregulation in cancer cells.

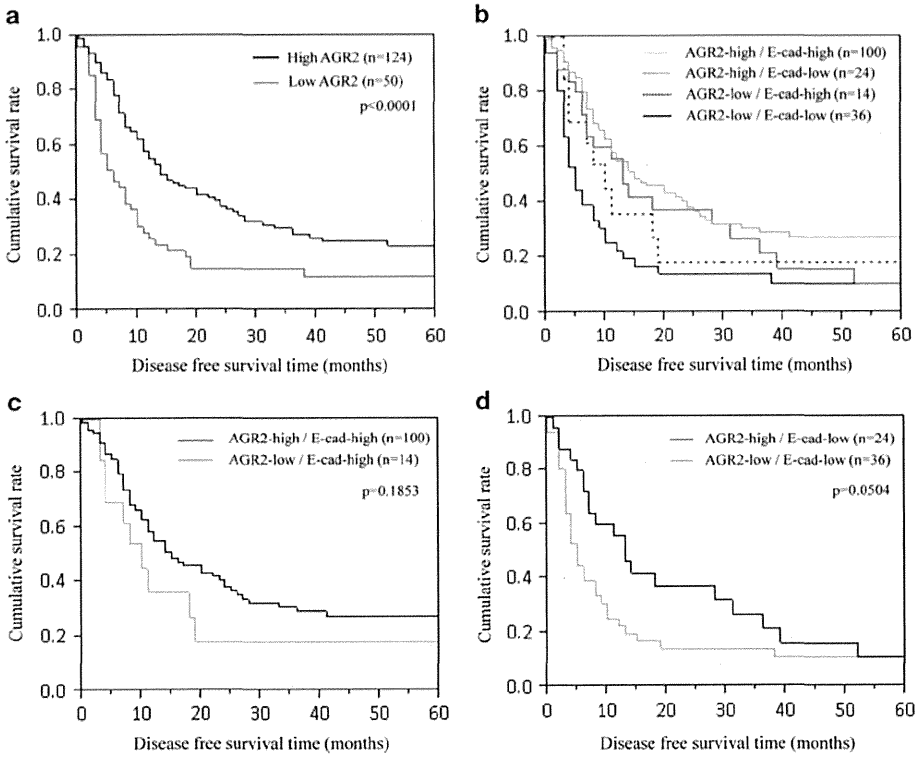

Figure 3 Kaplan–Meier survival curves demonstrating disease-free survival in PDAC patients according to anterior gradient 2 (AGR2) and E-cadherin expression. Low AGR2 expression was associated with poor prognosis in disease-free survival (**a**; log-rank test; $P<0.0001$). Disease-free survival rate with combined AGR2 and E-cadherin status (**b**). In both high- and low-E-cadherin expression cohorts, low AGR2 expression was associated with a lower survival rate (**c** and **d**).

AGR2 Downregulation Mediated by TGF-β Signaling Secreted by PSCs

TGF-β has previously been described as an inducer of EMT[33] and a negative regulator of AGR2[34] in PDAC. We next examined total levels of secreted TGF-β in co-culture supernatants of Aspc-1 and PSCs by ELISA. Whereas low levels of TGF-β were secreted into the medium of Aspc-1 monocultures, the concentration of TGF-β in co-culture supernatants was 2.5–4.5-fold higher ($\approx$1 ng/ml, Figure 6e). AGR2 expression was decreased following treatment of Panc-1, Aspc-1, and Capan-2 cells with human recombinant TGF-β1. High levels of EGF also inhibited AGR2 expression in Aspc-1 and Capan-2 cells, but not in Panc-1 cells, whereas treatment with FGF-2 did not alter AGR2 expression in PDAC cells (Figure 6f). In addition, the level of phosphorylated ERK1/2 was elevated in cancer cells co-cultured with PSCs compared with monocultures. Phosphorylated Smad2/3 was observed in Panc-1 and Capan-2 cells, but not in Aspc-1 cells (Figure 6d). AGR2 downregulation was associated with phosphorylation of ERK1/2 in Panc-1, Aspc-1, and Capan-2 cells. To confirm whether AGR2 expression is reduced by the function of TGF-β1 in PDAC cells, we performed co-culture experiments inhibiting TGF-β signaling using a TGF-β1 neutralizing antibody and recombinant human TGF-β receptor type II Fc Chimera. *AGR2* mRNA expression was restored in PDAC cells co-cultured with PSCs following inhibition of TGF-β signaling (Figure 6g). These results indicate that TGF-β secreted from PSCs may partially contribute to downregulation of AGR2.

DISCUSSION

In this study, we demonstrated that AGR2 downregulation occurred in high histological grade PDAC in association with EMT induction, and correlated with poor outcome in PDAC patients. We also demonstrated that AGR2 expression was downregulated in PDAC cells following co-culture with PSCs, consistent with EMT induction, and TGF-β1 secreted from PSCs partially contribute to its AGR2 downregulation.

Our IHC analyses revealed that AGR2 expression was upregulated during neoplastic initiation and subsequently downregulated during cancer progression, cancer cell de-differentiation, and EMT induction. This suggests that AGR2 may contribute to early neoplastic initiation by increasing proliferation and migration rather than progression and metastasis, and that downregulation of AGR2 occurs in advanced- and high-grade PDAC. IHC analyses of EMT markers in these specimens also demonstrated that AGR2 downregulation was correlated with EMT induction in

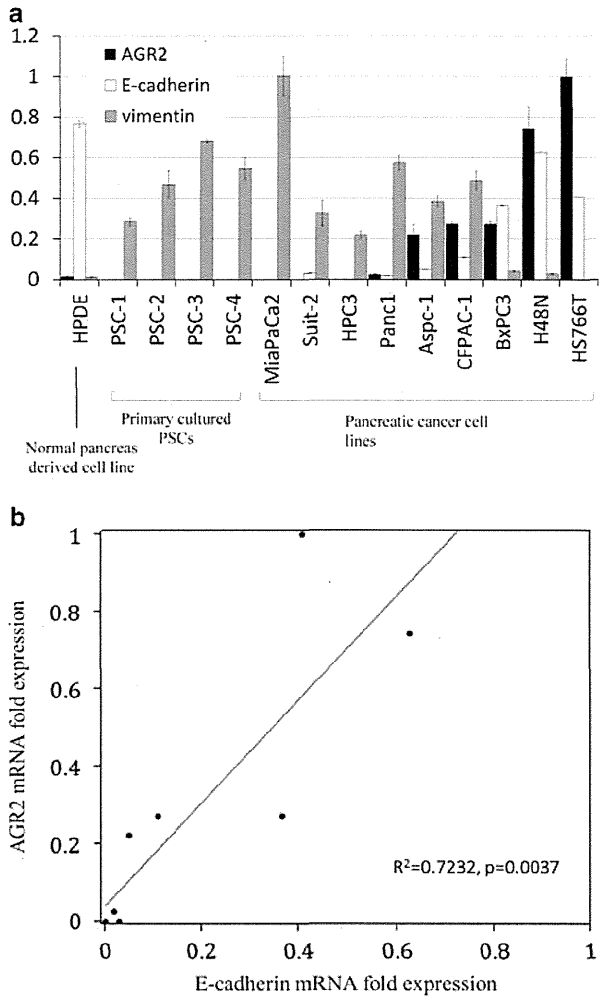

Figure 4 Quantitative reverse transcription-PCR for anterior gradient 2 (*AGR2*) expression in pancreatic cancer cell lines. *AGR2* expression differed in the various pancreatic cancer cell lines. High *AGR2*-expressing cell lines exhibited overexpression of vimentin and reduced E-cadherin expression. Epithelial-type cancer cells (HS766T, H48N, and BxPC-3), retained cellular adhesiveness and *AGR2* expression, whereas mesenchymal-type cancer cell lines (MiaPaCa2, SUIT-2, and HPC-3) exhibiting spindle-shaped morphology expressed low levels of *AGR2*. *AGR2* and E-cadherin expression was very low and vimentin expression was quite high in the primary-cultured pancreatic stellate cells (PSCs) (**a**). Linear regression analysis demonstrated a strong positive correlation between AGR2 and E-cadherin messenger RNA (mRNA) levels (**b**: $R^2 = 0.7262$, $P = 0.0035$).

PDAC patients. In this study, AGR2 downregulation occurred in only 28% of PDAC patients. It should be noted that AGR2 expression can also be upregulated in PDAC, as other publications have suggested.[14,16]

Previous reports have documented conflicting results regarding the prognostic value of AGR2 expression. In prostate cancer tissue, AGR2 downregulation correlated with increased Gleason grade, a histological grading system of prostate cancer, and increased cancer recurrence in Gleason grades 4 or 5.[35] A more recent report demonstrated that high AGR2 expression and low CD10 expression were favorable prognostic markers in prostate cancer.[36] In contrast, another reported that increased AGR2 expression was correlated with poorer outcome in prostate cancer.[13] Similar controversy regarding the prognostic value of AGR2 expression has been observed in breast cancer; with AGR2 upregulation associated with favorable prognosis in one study,[37] and with poor prognosis in another independent analysis.[11]

Previous studies of PDAC did not identify a correlation between AGR2 expression and prognosis.[15] Our univariate analysis revealed that AGR2 downregulation correlated with poor prognosis in PDAC patients. In contrast, multivariate analysis revealed that AGR2 expression was not a poor prognostic marker, whereas downregulation of E-cadherin had significant prognostic value (Supplementary Table 2). Furthermore, division of patients into two groups based on E-cadherin expression reveals that low-AGR2 expression tends to be an indicator of shorter survival, although this difference was not statistically significant (Figures 3c and d). It can be said that AGR2 has a strong correlation with E-cadherin and makes it as a strong confounding factor. Indeed, exclusion of E-cadherin expression from the multivariate analysis revealed that AGR2 downregulation was an independent prognostic marker (data not shown), suggesting the strong correlation between AGR2 downregulation and decreased membranous E-cadherin expression. In the view of a prognostic marker, as AGR2 is secreted into the pancreatic fluid, unlike E-cadherin or vimentin,[38] it may represent a useful and convenient pre-operative prognostic marker. To the best of our knowledge, our study is the first report demonstrating the prognostic significance of decreased AGR2 expression in PDAC patients.

Whereas AGR2 has been previously described as an oncoprotein capable of promoting cancer cell proliferation, invasiveness, and migration in various PDAC cell lines,[14] our IHC study revealed that AGR2 was downregulated during PDAC progression and this was associated with poor prognosis. Consistent with our IHC results in PDAC, recent reports reveal that AGR2 immunoreactivity is frequently lost in colorectal carcinoma, and may represent a novel prognostic indicator for overall patient survival.[39]

Discrepancy between pro-oncogenic function of AGR2 as previously reported and the prognostic significance of AGR2 downregulation may have several explanations. First, the biological outcome of altered AGR2 expression may depend on the origin of tumor development. For example, caveolin-1, an essential constituent protein of specialized membrane invaginations referred to as caveolae, was upregulated in prostate cancer tissue,[40] but downregulated in colon cancer tissue.[41] Targeted knockdown of AGR2 in PDAC cells using siRNA revealed that AGR2 silencing suppressed the proliferation, invasiveness, and migration of Aspc-1 and Hs766T cells, as previously reported in other PDAC cell lines (BxPC-3, SU8686, CFPAC-1, and MPanc-96),[14] but did not alter EMT markers. These data suggest that AGR2 promotes cancer

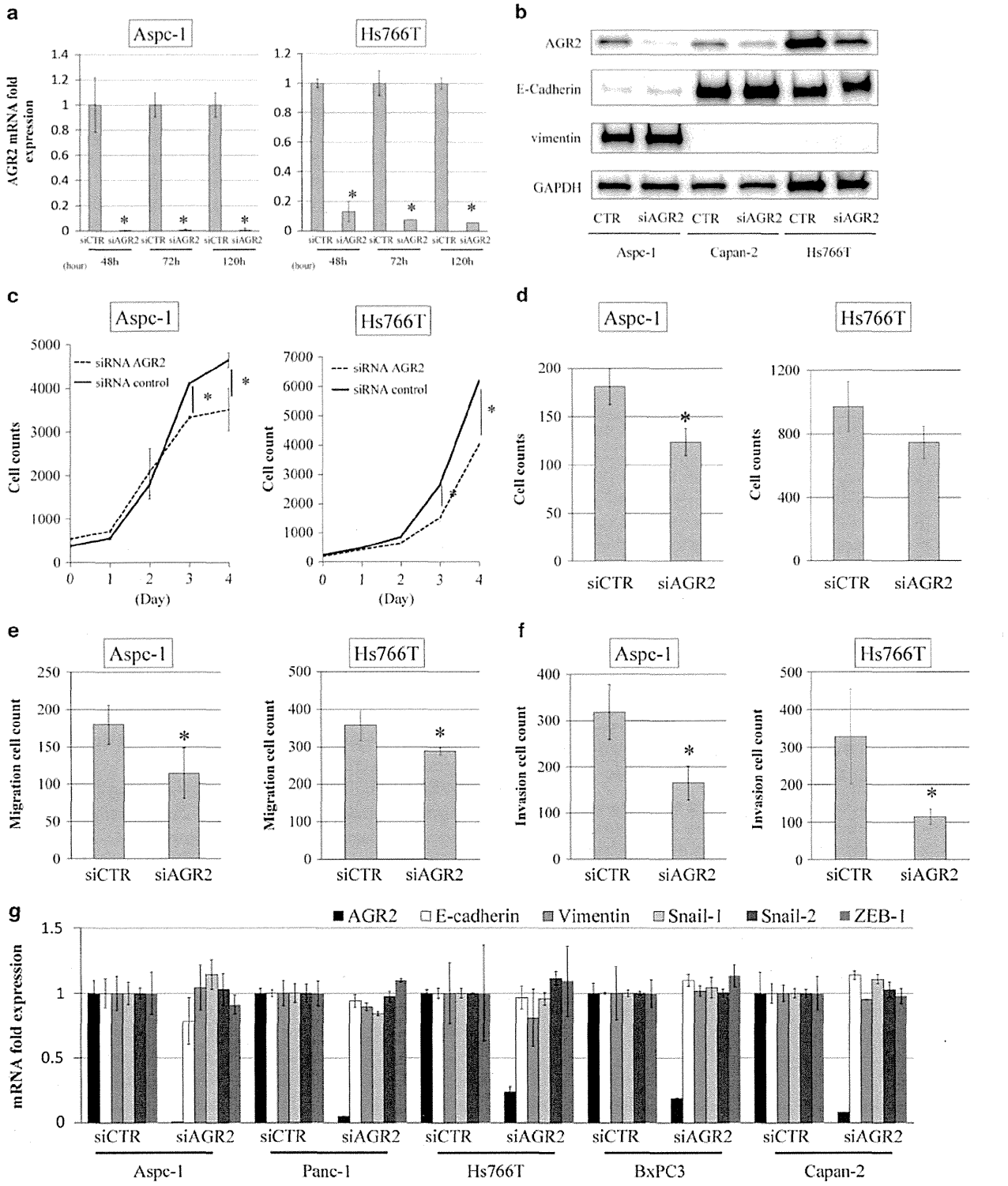

Figure 5 Targeted inhibition of anterior gradient 2 (AGR2) using small-interfering RNA (siRNA). AGR2 silencing was confirmed following transfection of Aspc-1 and Hs766T cells with AGR2-specific siRNA by quantitative reverse transcription (qRT)-PCR (**a**) 48, 72, and 120 h, and immunoblot analysis 72 h post transfection, respectively (**b**). E-cadherin and vimentin expression levels were not altered by AGR2 knockdown as assessed by immunoblot analysis (**b**). AGR2 knockdown significantly reduced cell proliferation (**c**), colony formation (**d**), cell migration (**e**), and cell invasiveness (**f**) in Aspc-1 and Hs766T cells ($P<0.01$), except for the colony formation assay in Hs766T cells ($P=0.0686$). AGR2 knockdown did not alter messenger RNA (mRNA) levels of epithelial–mesenchymal transition markers, E-cadherin, vimentin, Snail-1, Snail-2, and ZEB-1 (**g**). Data represent the mean values of triplicate experiments (*$P<0.01$, *versus* control). GAPDH, glyceraldehyde 3-phosphate dehydrogenase.

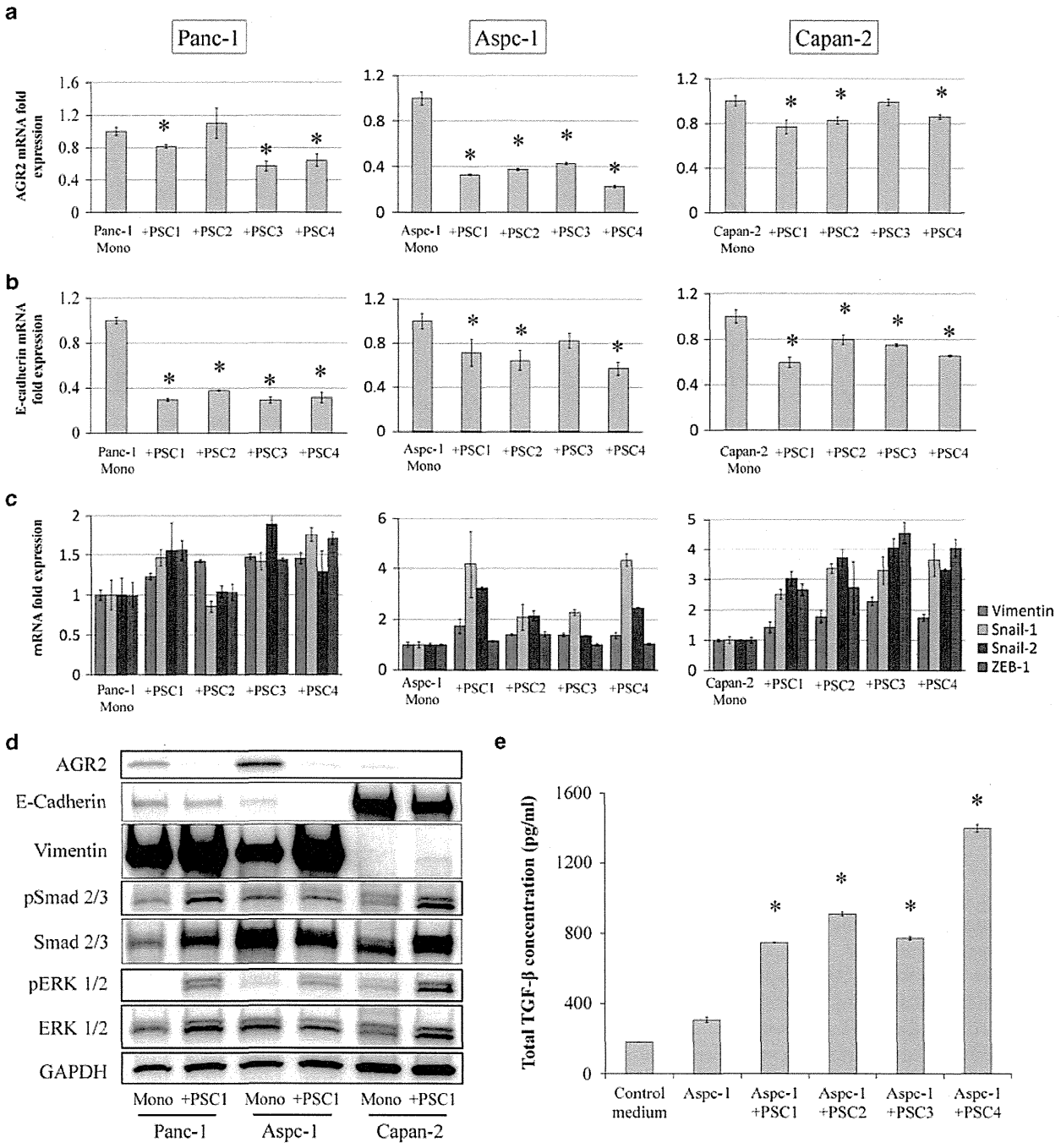

Figure 6 Indirect co-culture experiment of pancreatic ductal adenocarcinoma (PDAC) cells with pancreatic stellate cell (PSCs) and treatment with recombinant growth factors. Anterior gradient 2 (AGR2) expression was decreased in PDAC cells co-cultured with PSCs using an indirect co-culture system (**a**) in accordance with epithelial–mesenchymal transition induction (E-cadherin downregulation (**b**) and overexpression of vimentin, Snail-1, Snail-2 and ZEB-1 (**c**)) by quantitative reverse transcription-PCR (*$P<0.01$, *versus* monocultures). Decreased expression of AGR2 was observed in co-cultured cancer cells compared with monocultures. Decreased AGR2 expression was also associated with increased levels of phosphorylated Smad2/3 and ERK1/2, with the exception of phosphorylated Smad2/3 in Aspc-1 (**d**). E-cadherin and vimentin expression were also slightly altered at the protein level (**d**). Enzyme-linked immunosorbent assays revealed that total, secreted transforming growth factor beta-1 (TGF-β1) levels were higher in co-culture supernatants than that of monocultures (**e**: *$P<0.001$, *versus* the medium of Aspc-1 monocultures). Treatment with recombinant proteins showed that reduced expression of AGR2 was observed by TGF-β1 in all PDAC cells examined and by high-dose epidermal growth factor (EGF) in Aspc-1 and Capan-2 cells (**f**). AGR2 expression was decreased by TGF-β1 or co-cultured with PSCs, and restored by inhibition of TGF-β signaling (**g**). Data represent the mean values of triplicate experiments (*$P<0.01$, *versus* control). GAPDH, glyceraldehyde 3-phosphate dehydrogenase; FGF-2, fibroblast growth factor 2; mRNA, messenger RNA.

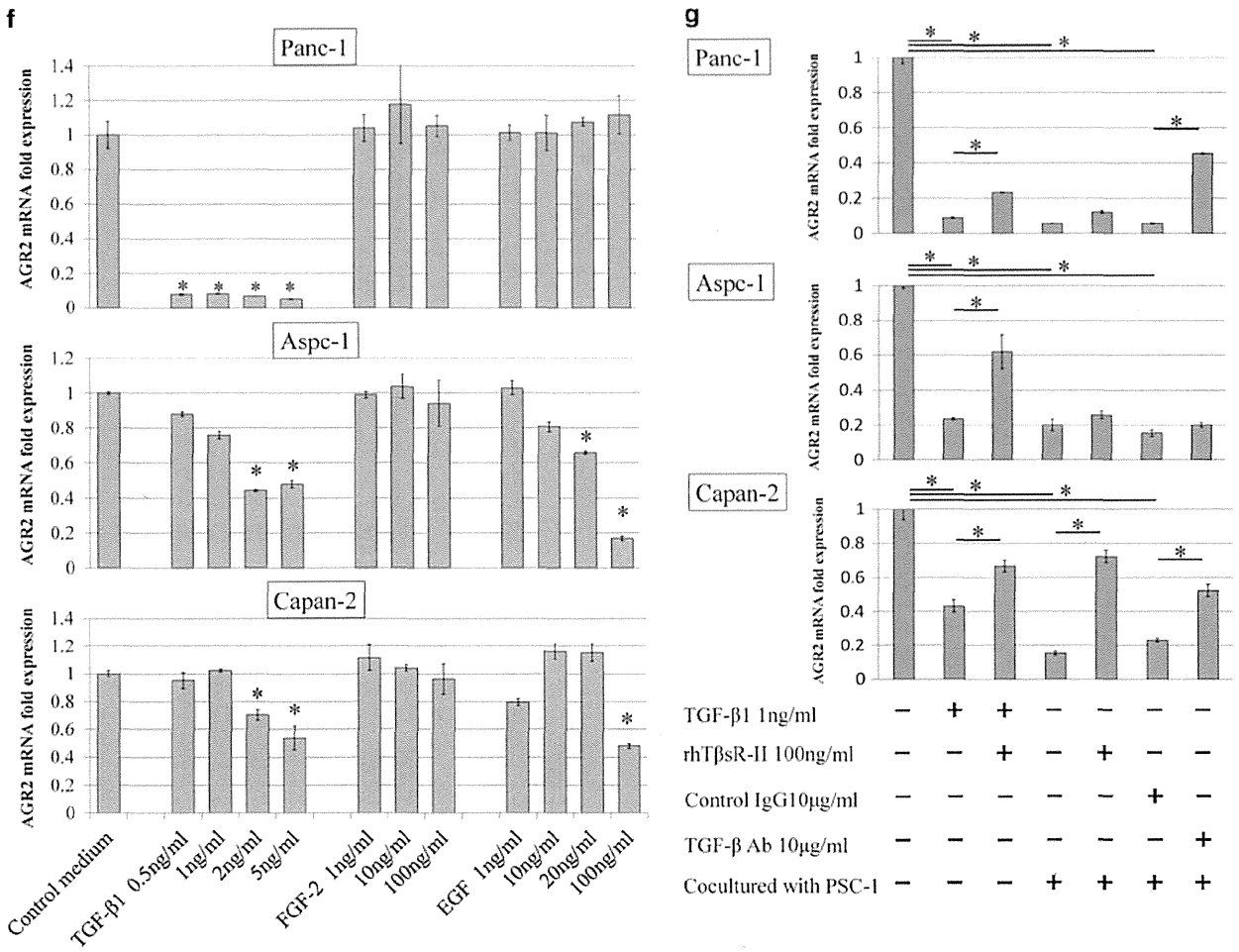

Figure 6 Continued.

progression, but does not induce EMT or mesenchymal–epithelial transition in PDAC patients. Second, the effect of AGR2 expression may also be dependent on tumor stage. IHC analyses revealed that AGR2 was expressed in precursor PDAC lesions, and its expression was higher than in PDAC. It was proposed that the pro-oncogenic function of AGR2 may be active during early tumor development and promote neoplastic initiation, with TGF-β secreted from PSCs in the cancer stroma functioning as an upstream negative regulator of AGR2 at the late stage of cancer progression. Thus, it was suggested that the oncogenic function of AGR2 exerted little influence on prognosis in PDAC patients. Third, AGR2 downregulation in PDAC was caused by morphological and phenotypic alterations during pancreatic cancer progression. We demonstrated that AGR2 expression was decreased in parallel with EMT induction, characterized by decreased membranous E-cadherin expression and increased cytoplasmic vimentin expression in IHC analyses. On the basis of these observations, we hypothesized that AGR2 downregulation may be mediated by upstream regulators that function as EMT inducers.

PSCs are one of the most important cell populations in the pancreatic cancer stroma. PSCs are also observed surrounding PanIN lesions; however, it has been reported that the cellular density of PSCs is lower than that of PDAC, and that the phenotypic characteristics of PSCs surrounding PanINs may be different from that in PDAC.[42] As cancer cells invade the stroma, destructing the basement membrane, they interact with stromal cells including PSCs. This interaction promotes tumor formation and metastasis induced by secreted soluble factors from stromal cells, including various growth factors and cytokines. Whereas AGR2 itself promotes cancer initiation in PDAC development, it was suggested that other pro-oncogenic factors secreted from cancer microenvironments also contribute to cancer cell invasiveness. AGR2 expression was consequently reduced following induction of EMT (alteration to mesenchymal morphology) and the acquisition of a highly aggressive phenotype by these secreted factors. To identify such soluble factors associated with AGR2 downregulation in PDAC cells, we cultured PDAC cells with culture medium containing various recombinant growth factors known as EMT-inducible factors and secreted from

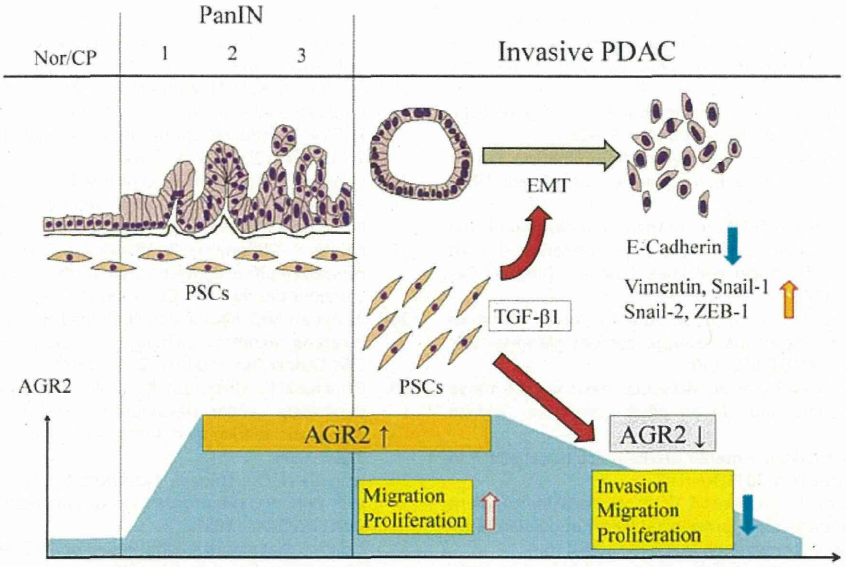

Figure 7 Schematic summarising the mechanisms of anterior gradient 2 (AGR2) downregulation. AGR2 expression was not observed in non-neoplastic epithelium of normal pancreas or chronic pancreatitis, but was upregulated in intraepithelial neoplastic lesions and contributed to cancer development. As cancer cells invade the stroma through the basement membrane, EMT is induced following interaction with stromal cells, including PSCs. AGR2 is downregulated by TGF-β1 secreted from PSCs. Cancer progression is slightly reduced by AGR2 downregulation; however, the various oncogenic factors, upregulated in advanced PDAC, retain or promote cancer progression. (Nor/CP, pancreatic ductal epithelium of normal pancreas and chronic pancreatitis; PanIN, pancreatic intraepithelial epithelium; PDAC, pancreatic ductal adenocarcinoma; EMT, epithelial–mesenchymal transition; PSCs, pancreatic stellate cells; TGF-β1, transforming growth factor beta-1).

PSCs, suggesting that AGR2 downregulation may occur in advanced PDAC cells by this factor secreted from PSCs in cancer stroma.

A recent study demonstrated that AGR2 expression is suppressed in Panc-1 cells with wild-type Smad4 by a canonical TGF-β/Smad signaling pathway;[34] however, our study revealed that TGF-β treatment reduced AGR2 expression in not only Capan-2 and Panc-1, but also Aspc-1 cells harboring *Smad4* mutation.[43] The concentration of TGF-β in cell supernatants co-cultured with PSCs, as assessed by ELISA, was $\approx$1000 pg/ml. Importantly, this level was sufficient to mediate AGR2 downregulation. TGF-β also stimulates phosphorylation of ERK1/2 through a Smad-independent pathway.[44] Co-culture experiments demonstrated that phosphorylation of ERK1/2 occurred in parallel with AGR2 downregulation. This suggests that TGF-β signaling was activated in the PDAC co-culture setting regardless of DPC4 mutation, and TGF-β-mediated downregulation of AGR2 also occurs via a Smad-independent pathway, although the exact mechanism(s) underlying the downregulation of AGR2 by TGF-β signaling remains unclear. These results are schematically summarized in Figure 7.

Collectively, although the complete mechanisms of AGR2 downregulation accompanying EMT induction remain unclear, we demonstrated that AGR2 is downregulated in PDAC compared with pre-malignant lesions, and AGR2 expression may be a favorable prognostic marker. Targeted silencing of AGR2 using siRNA revealed that AGR2 promotes cancer cell proliferation, migration, and invasion, confirming previous reports that AGR2 itself functions as an oncoprotein. Reduced AGR2 expression was detected in PDAC cell lines co-cultured with primary-cultured PSC, in parallel with EMT induction. These results suggest that reduced AGR2 expression does not cause EMT, but is the result of aggressive phenotype in advanced PDAC.

Supplementary Information accompanies the paper on the Laboratory Investigation website (http://www.laboratoryinvestigation.org)

ACKNOWLEDGMENTS

We thank N Tateishi (Department of Anatomic Pathology, Kyushu University Hospital) and E Manabe (Department of Surgery and Oncology, Kyushu University Hospital) for their expert technical assistance. This study was supported by a Grant-in-Aid for the Japan Society for the Promotion of Science Fellows (13-3401). We also thank Edanz Group Japan for revising the English used in this article.

DISCLOSURE/CONFLICT OF INTEREST

The authors declare no conflict of interest.

1. Siegel R, Naishadham D, Jemal A. Cancer statistics, 2012. CA Cancer J Clin 2012;62:10–29.
2. Hruban RH, Wilentz RE, Kern SE. Genetic progression in the pancreatic ducts. Am J Pathol 2000;156:1821–1825.

3. van Heek T, Rader AE, Offerhaus GJ, *et al.* K-ras, p53, and DPC4 (MAD4) alterations in fine-needle aspirates of the pancreas: a molecular panel correlates with and supplements cytologic diagnosis. Am J Clin Pathol 2002;117:755–765.
4. Hansel DE, Kern SE, Hruban RH. Molecular pathogenesis of pancreatic cancer. Annu Rev Genomics Hum Genet 2003;4:237–256.
5. Sive HL, Hattori K, Weintraub H. Progressive determination during formation of the anteroposterior axis in Xenopus laevis. Cell 1989; 58:171–180.
6. Thompson DA, Weigel RJ. HAG-2, the human homologue of the Xenopus laevis cement gland gene XAG-2, is coexpressed with estrogen receptor in breast cancer cell lines. Biochem Biophys Res Commun 1998;251:111–116.
7. Aberger F, Weidinger G, Grunz H, *et al.* Anterior specification of embryonic ectoderm: the role of the Xenopus cement gland-specific gene XAG-2. Mech Dev 1998;72:115–130.
8. Kumar A, Godwin JW, Gates PB, *et al.* Molecular basis for the nerve dependence of limb regeneration in an adult vertebrate. Science 2007;318:772–777.
9. Brychtova V, Vojtesek B, Hrstka R. Anterior gradient 2: a novel player in tumor cell biology. Cancer Lett 2011;304:1–7.
10. Darb-Esfahani S, Fritzsche F, Kristiansen G, *et al.* Anterior gradient protein 2 (AGR2) is an independent prognostic factor in ovarian high-grade serous carcinoma. Virchows Arch 2012;461:109–116.
11. Innes HE, Liu D, Barraclough R, *et al.* Significance of the metastasis-inducing protein AGR2 for outcome in hormonally treated breast cancer patients. Br J Cancer 2006;94:1057–1065.
12. Wang Z, Hao Y, Lowe AW. The adenocarcinoma-associated antigen, AGR2, promotes tumor growth, cell migration, and cellular transformation. Cancer Res 2008;68:492–497.
13. Zhang Y, Forootan SS, Liu D, *et al.* Increased expression of anterior gradient-2 is significantly associated with poor survival of prostate cancer patients. Prostate Cancer Prostatic Dis 2007;10:293–300.
14. Ramachandran V, Arumugam T, Wang H, *et al.* Anterior gradient 2 is expressed and secreted during the development of pancreatic cancer and promotes cancer cell survival. Cancer Res 2008;68:7811–7818.
15. Riener MO, Pilarsky C, Gerhardt J, *et al.* Prognostic significance of AGR2 in pancreatic ductal adenocarcinoma. Histol Histopathol 2009;24: 1121–1128.
16. Dumartin L, Whiteman HJ, Weeks ME, *et al.* AGR2 is a novel surface antigen that promotes the dissemination of pancreatic cancer cells through regulation of cathepsins B and D. Cancer Res 2011;71:7091–7102.
17. Hugo H, Ackland ML, Blick T, *et al.* Epithelial—mesenchymal and mesenchymal—epithelial transitions in carcinoma progression. J cell Physiol 2007;213:374–383.
18. Prudkin L, Liu DD, Ozburn NC, *et al.* Epithelial-to-mesenchymal transition in the development and progression of adenocarcinoma and squamous cell carcinoma of the lung. Mod Pathol 2009;22: 668–678.
19. Morali OG, Delmas V, Moore R, *et al.* IGF-II induces rapid beta-catenin relocation to the nucleus during epithelium to mesenchyme transition. Oncogene 2001;20:4942–4950.
20. Jeong H, Ryu YJ, An J, *et al.* Epithelial-mesenchymal transition in breast cancer correlates with high histological grade and triple-negative phenotype. Histopathology 2012;60:E87–E95.
21. Bachem MG, Schneider E, Gross H, *et al.* Identification, culture, and characterization of pancreatic stellate cells in rats and humans. Gastroenterology 1998;115:421–432.
22. Erkan M, Adler G, Apte MV, *et al.* StellaTUM: current consensus and discussion on pancreatic stellate cell research. Gut 2012;61:172–178.
23. Hwang RF, Moore T, Arumugam T, *et al.* Cancer-associated stromal fibroblasts promote pancreatic tumor progression. Cancer Res 2008;68:918–926.
24. Miettinen PJ, Ebner R, Lopez AR, *et al.* TGF-beta induced transdifferentiation of mammary epithelial cells to mesenchymal cells: involvement of type I receptors. J Cell Biol 1994;127:2021–2036.
25. Sakuma K, Aoki M, Kannagi R. Transcription factors c-Myc and CDX2 mediate E-selectin ligand expression in colon cancer cells undergoing EGF/bFGF-induced epithelial-mesenchymal transition. Proc Natl Acad Sci USA 2012;109:7776–7781.
26. El-Hariry I, Pignatelli M, Lemoine NR. FGF-1 and FGF-2 regulate the expression of E-cadherin and catenins in pancreatic adenocarcinoma. Int J Cancer 2001;94:652–661.
27. Kikuta K, Masamune A, Watanabe T, *et al.* Pancreatic stellate cells promote epithelial-mesenchymal transition in pancreatic cancer cells. Biochem Biophys Res Commun 2010;403:380–384.
28. Al-Aynati MM, Radulovich N, Riddell RH, *et al.* Epithelial-cadherin and b-catenin expression changes in pancreatic intraepithelial neoplasia. Clin Cancer Res 2004;10:1235–1240.
29. Ohuchida K, Mizumoto K, Ishikawa N, *et al.* The role of S100A6 in pancreatic cancer development and its clinical implication as a diagnostic marker and therapeutic target. Clin Cancer Res 2005;11: 7785–7793.
30. Ikenaga N, Ohuchida K, Mizumoto K, *et al.* CD10 + pancreatic stellate cells enhance the progression of pancreatic cancer. Gastroenterology 2010;139:1041–1051.
31. Odate S, Nakamura K, Onishi H, *et al.* TrkB/BDNF signaling pathway is a potential therapeutic target for pulmonary large cell neuroendocrine carcinoma. Lung Cancer 2013;79:205–214.
32. Tsang ML, Zhou L, Zheng BL, *et al.* Characterization of recombinant soluble human transforming growth factor-beta receptor type II (rhTGF-beta sRII). Cytokine 1995;7:389–397.
33. Ellenrieder V, Hendler SF, Boeck W, *et al.* Transforming growth factor beta1 treatment leads to an epithelial-mesenchymal transdifferentiation of pancreatic cancer cells requiring extracellular signal-regulated kinase 2 activation. Cancer Res 2001;61:4222–4228.
34. Norris AM, Gore A, Balboni A, *et al.* AGR2 is a SMAD4-suppressible gene that modulates MUC1 levels and promotes the initiation and progression of pancreatic intraepithelial neoplasia. Oncogene 2013;32:3867–3876.
35. Maresh EL, Mah V, Alavi M, *et al.* Differential expression of anterior gradient gene AGR2 in prostate cancer. BMC Cancer 2010;10:680.
36. Ho ME, Quek SI, True LD, *et al.* Prostate cancer cell phenotypes based on AGR2 and CD10 expression. Mod Pathol 2013;26:849–859.
37. Fritzsche FR, Dahl E, Pahl S, *et al.* Prognostic relevance of AGR2 expression in breast cancer. Clin Cancer Res 2006;12:1728–1734.
38. Chen R, Pan S, Duan X, *et al.* Elevated level of anterior gradient-2 in pancreatic juice from patients with pre-malignant pancreatic neoplasia. Mol Cancer 2010;9:149.
39. Riener MO, Thiesler T, Hellerbrand C, *et al.* Loss of Anterior gradient-2 expression is an independent prognostic factor in colorectal carcinomas. Eur J Cancer 2014;50:1722–1730.
40. Yang G, Truong LD, Wheeler TM, *et al.* Caveolin-1 expression in clinically confined human prostate cancer: a novel prognostic marker. Cancer Res 1999;59:5719–5723.
41. Bender FC, Reymond MA, Bron C, *et al.* Caveolin-1 levels are down-regulated in human colon tumors, and ectopic expression of caveolin-1 in colon carcinoma cell lines reduces cell tumorigenicity. Cancer Res 2000;60:5870–5878.
42. Shi C, Washington MK, Chaturvedi R, *et al.* Fibrogenesis in pancreatic cancer is a dynamic process regulated by macrophage-stellate cell interaction. Lab Invest 2014;94:409–421.
43. Schutte M, Hruban RH, Hedrick L, *et al.* DPC4 gene in various tumor types. Cancer Res 1996;56:2527–2530.
44. Zavadil J, Bitzer M, Liang D, *et al.* Genetic programs of epithelial cell plasticity directed by transforming growth factor-beta. Proc Natl Acad Sci USA 2001;98:6686–6691.

Clinical Significance of *GNAS* Mutation in Intraductal Papillary Mucinous Neoplasm of the Pancreas With Concomitant Pancreatic Ductal Adenocarcinoma

Noboru Ideno, MD, Takao Ohtsuka, MD, PhD,* Taketo Matsunaga, MD,* Hideyo Kimura, MD,* Yusuke Watanabe, MD,* Koji Tamura, MD,* Teppei Aso, MD,* Shinichi Aishima, MD, PhD,† Yoshihiro Miyasaka, MD, PhD,* Kenoki Ohuchida, MD, PhD,* Junji Ueda, MD, PhD,* Shunichi Takahata, MD, PhD,* Yoshinao Oda, MD, PhD,† Kazuhiro Mizumoto, MD, PhD,* and Masao Tanaka, MD, PhD, FACS**

Objective: The aims of this study were to investigate the *GNAS* mutational status in pancreatic intraductal papillary mucinous neoplasm (IPMN) with and without distinct pancreatic ductal adenocarcinoma (PDAC) and to evaluate the significance of *GNAS* analysis using duodenal fluid (DF) in patients with IPMN.

Methods: The clinicopathologic features of 110 patients with IPMN including 16 with distinct PDAC were reviewed. The *GNAS* status in the IPMN tissue and 23 DF specimens was assessed by sensitive mutation scanning methods.

Results: The *GNAS* mutation rate in IPMN with distinct PDAC was significantly lower than that in IPMN without PDAC (4/16, 25%, vs 61/94, 65%; $P = 0.0047$). By multivariate analysis, *GNAS* wild-type and gastric type IPMNs were significantly associated with distinct PDAC. Of 45 *GNAS* wild-type IPMNs, 10 (43%) of 23 gastric type IPMNs had distinct PDAC, whereas only 2 (9%) of 22 non–gastric type IPMNs had distinct PDAC ($P = 0.017$). The *GNAS* status in DF was consistent with that in tissue in 21 (91%) of 23 patients.

Conclusions: Distinct PDACs frequently develop in the pancreas with gastric type IPMN without *GNAS* mutations. Duodenal fluid DNA test would predict the *GNAS* status of IPMN, whereas the detection of the gastric subtype using noninvasive test remains to be determined.

Key Words: intraductal papillary mucinous neoplasm of the pancreas, pancreatic ductal adenocarcinoma, *GNAS* mutation

(*Pancreas* 2015;44: 311–320)

Pancreatic ductal adenocarcinoma (PDAC) is a major cause of cancer-related death worldwide, with a mortality rate of greater than 95%.[1] Screening for asymptomatic high-risk individuals and detection of early-stage PDAC, ideally noninvasive PDAC, followed by surgical resection are currently considered to be the only way to cure patients with PDAC because most patients with symptomatic invasive PDAC die of recurrence due to the high malignant potential.[2]

From the *Departments of Surgery and Oncology, and †Anatomic Pathology, Graduate School of Medical Sciences, Kyushu University, Fukuoka, Japan.
Received for publication December 25, 2013; accepted July 1, 2014.
Reprints: Masao Tanaka, MD, PhD, FACS, Department of Surgery and Oncology, Graduate School of Medical Sciences, Kyushu University, 3-1-1 Maidashi, Higashi-ku, Fukuoka 812-8582, Japan (e-mail: masaotan@med.kyushu-u.ac.jp).
This study was supported in part by a Grant-in-Aid from the Ministry of Education, Culture, Sports, Science and Technology of Japan (Grant No. 25293285).
The authors declare no conflict of interest.
Supplemental digital contents are available for this article. Direct URL citations appear in the printed text and are provided in the HTML and PDF versions of this article on the journal's Web site (www.pancreasjournal.com).

Intraductal papillary mucinous neoplasm (IPMN) of the pancreas is a precursor to invasive carcinoma, and its characteristics of slow and nonaggressive growth provide an opportunity for curative resection.[3,4] Although branch duct IPMN (BD-IPMN) can be essentially watched until it shows high-risk stigmata of malignancy or worrisome features defined in the international consensus guidelines of IPMN, several recent reports have demonstrated that malignant character can be observed even in small and flat BD-IPMN.[5,6] In addition, most PDACs concomitant with IPMN are still found in the advanced stage during management of such benign-looking BD-IPMNs.[7–17] Therefore, the identification of predictors with value in terms of personalized approaches to the management of patients with IPMN is urgent.

The Johns Hopkins group has recently shown that the mutation of *GNAS*, a gene encoding the guanine nucleotide–binding protein (G-protein) α subunit (Gsα), was observed in 61% of resected IPMNs, and the detection of *GNAS* mutation in cystic fluid is reported to be useful to distinguish IPMN from other cystic neoplasms.[18–20] Our previous study revealed that distinct PDAC was frequently observed in patients with benign gastric type IPMNs.[14] In addition, *GNAS* mutation within codon 201 was absent in all 5 examined gastric type IPMN specimens.[14] Therefore, evaluation of the *GNAS* gene in IPMN might be useful to identify individuals at high risk for the development of distinct PDAC. However, the detection rate of *GNAS* mutation seems to differ according to the mutation scanning technology used; thus, our results should be validated by sensitive methods with larger case series.

Several DNA tests for the diagnosis of pancreatic diseases using duodenal fluid (DF) have been reported.[21–23] Kanda et al[22] showed that the detection rate of *GNAS* mutation in DF including pancreatic juice in patients radiographically diagnosed as IPMN was 64%, which is quite similar to the rate observed in resected IPMN specimens. Therefore, DF testing has the potential to predict the mutational status of *GNAS* in patients with IPMN. Comparative analysis of the *GNAS* status between a DF specimen and a resected IPMN specimen in a given individual with distinct PDAC would help to indicate the clinical significance of the detection of *GNAS* mutation in DF. The aims of this study were to investigate the *GNAS* mutational status in IPMN with and without distinct PDAC in a large consecutive series using sensitive mutation scanning methods and to evaluate the role of *GNAS* gene analysis in preoperatively collected DF for the management of IPMN.

MATERIALS AND METHODS

This study was approved by the Ethics Committee of Kyushu University and conducted according to the Ethical Guidelines for Analytical Research of the Human Genome/Genes enacted by the Japanese government and the Helsinki Declaration.

Patients and Specimens

A total of 121 consecutive patients underwent resection of IPMN at Kyushu University Hospital between February 2005 and January 2013. Formalin-fixed, paraffin-embedded (FFPE) resected IPMN specimens were obtained from all patients. Among them, the DNA quality was insufficient for mutation analyses in 11 patients; therefore, the data were available in the remaining 110 patients. Histopathologic grades and subtypes of IPMN were assessed according to the World Health Organization classification system of 2010.[24] Of these 110 patients, 25 had invasive carcinoma derived from IPMN, and the remaining 85 had noninvasive IPMN, including 42 with low-grade dysplasia (LGD), 21 with intermediate-grade dysplasia (IGD), and 22 with high-grade dysplasia (HGD) (Table 1). Invasive carcinomas were carefully examined for the presence or absence of a transitional area from intraductal epithelial dysplasia to invasive carcinoma to discriminate invasive carcinoma derived from IPMN from PDAC distinct from IPMN. Invasive carcinomas with this transitional area were diagnosed as invasive carcinoma derived from IPMN, whereas those without the transitional area were diagnosed as PDAC concomitant with IPMN.[14,15,17] Of all 110 patients, 16 (15%) had PDAC concomitant with IPMN, and the histopathologic grade of the coexisting IPMN was LGD in 8 patients, IGD in 5, HGD in 2, and invasive IPMN in 1. In 7 of these 16 patients with PDAC concomitant with IPMN, *GNAS/KRAS* mutation status of both IPMN and concomitant PDAC was analyzed by Sanger sequencing, and the data were reported in our previous article.[14] In the current study, the mutation status of these 7 cases was reevaluated by more sensitive mutation scanning methods including high-resolution melt curve (HRM) analysis and competitive allele-specific TaqMan polymerase chain reaction (PCR).

Duodenal fluid was prospectively collected at the time of preoperative endoscopic retrograde cholangiopancreatography (ERCP) for the patients with IPMN from April 2010 to January 2013 at our institution. The data of 5 patients were described in our previous report for another purpose.[25] After positioning the endoscope in the second portion of the duodenum, DF was collected for 5 minutes by gently pushing the duodenal mucosa using a StarTip ERCP cannula (PR130Q; Olympus Medical Systems Corp, Tokyo, Japan), as described in our previous report.[25] After DF collection, pancreatography and subsequent balloon catheter insertion into the main pancreatic duct were performed.[15] Pure pancreatic juice was collected after an intravenous administration of ChiRhoStim (1 μg per body; ChiRhoClin, Inc, Burtonsville, Md) for cytology. The collected DF and pancreatic juice were immediately aliquoted to 2-mL collection tubes and stored at −80°C until analysis.

Genomic DNA Extraction

Tumor tissues of both IPMN and invasive carcinoma with neoplastic cellularity of more than 50% were manually dissected from 10-μm sections of FFPE tissues, whereas those of invasive carcinoma with lower neoplastic cellularity were microscopically dissected[26] using a Leica LMD 6000 (Leica Microsystems, Wetzlar, Germany). The intraductal component of invasive carcinoma derived

TABLE 1. Comparative Analyses of Clinicopathologic Features and *GNAS/KRAS* Mutation Status Between IPMN With and Without Distinct PDAC

Variables		IPMN Without PDAC (n = 94)	IPMN With PDAC (n = 16)	*P*
Age	Median (range), y	70 (38–85)	68 (54–82)	0.89
Sex	Male	65 (69)	9 (56)	0.39
	Female	29 (31)	7 (44)	
Location of IPMN	Pancreatic head	54 (57)	12 (75)	0.27
	Other	40 (43)	4 (25)	
Morphological type	BD-IPMN	62 (66)	13 (81)	0.41
	Mixed-type IPMN	26 (28)	1 (6)	
	MD-IPMN	6 (6)	2 (13)	
Histopathologic grade of IPMN	LGD	34 (36)	8 (50)	0.4
	IGD	16 (17)	5 (31)	0.18
	HGD	20 (21)	2 (13)	0.52
	Invasive	24 (26)	1 (6)	0.11
Epithelial subtype	Gastric	52 (55)	12 (75)	0.18
	Intestinal	20 (21)	2 (13)	0.52
	Pancreatobiliary	20 (21)	2 (13)	0.52
	Oncocytic	2 (2)	0 (0)	1
Image branch duct size	Median (range), mm	30 (7–80)	23 (10–50)	0.11
Mural nodule	Present	41 (44)	4 (25)	0.18
	Absent	53 (56)	12 (75)	
GNAS mutation	Present	61 (65)	4 (25)	0.0047
	Absent	33 (35)	12 (75)	
KRAS mutation	Present	62 (66)	13 (81)	0.6
	Absent	18 (19)	2 (13)	
	Undetermined*	14 (15)	1 (6)	

The number in parentheses indicates the percentage of the total number of patients in each group.
*Positive result by high-resolution melt curve analysis and wild-type by Sanger sequencing.

from IPMN was selectively dissected. Genomic DNA was extracted using the QIAamp DNA FFPE Tissue Kit or QIAamp DNA Micro Kit (Qiagen, Hilden, Germany) according to the manufacturer's instructions.

The mean (SD) volume of DF obtained without secretin stimulation was 2.2 (1.7) mL, and sufficient genomic DNA could be extracted from 100 μL of DF specimens using the QIAamp DNA Micro Kit (Qiagen).

Detection of *GNAS* Mutation

GNAS is mutated in a wide variety of tumor types, and the vast majority of these mutations clusters around 2 hot spot residues, codons 201 and 227.[27] *GNAS* mutations in IPMN were reported to be present[19,28] only at codon 201; thus, we performed mutational analysis targeting codon 201.

An overview of the approach used for the detection of *GNAS* codon 201 mutation in the tissue specimens is presented in Figure 1. High-resolution melt curve analysis was initially performed to screen for the presence or absence of *GNAS* mutation in genomic DNA extracted from tissue specimens. The PCR products that were indicated to have *GNAS* mutation by HRM analysis were subjected to Sanger sequencing. When the specimens were indicated to be mutant by HRM analysis but wild-type by Sanger sequencing, they underwent competitive allele-specific TaqMan PCR (castPCR). Sanger sequencing can detect mutations at high concentrations of the mutant allele (approximately 25% or more), whereas HRM analysis and castPCR have detection limits of 5% to 10% and 0.1%, respectively.[29,30]

GNAS mutations in the DF samples were examined by castPCR because the ratio of the neoplastic cells to nonneoplastic cells such as duodenal epithelial cells and blood cells in DF was expected to be quite low according to previous articles.[21–23]

HRM Analysis

Polymerase chain reaction for HRM analysis was performed using 10 μL of solution in each well containing 10 ng of template genomic DNAs, 2 x SsoFast EvaGreen supermix (Bio-Rad Laboratories, Hercules, Calif), as well as 400 nmol/L of the forward and reverse primers listed in Supplemental Table 1, http://links.lww.com/MPA/A341. All specimens were tested in triplicate. In each PCR plate, 5 wells were allocated to wild-type control DNA and 1 well was allocated to no template control to validate the PCR. Polymerase chain reaction amplification was performed using the CFX 96 Real-Time PCR Detection System (Bio-Rad Laboratories), which included the following steps: initial denaturing at 95°C for 5 minutes, 50 cycles at 95°C for 30 seconds and 59°C for 30 seconds, as well as final denaturing at 95°C for 30 seconds and 28°C for 30 seconds to generate heteroduplexes. For HRM analysis, the PCR products were heated from 72°C to 96°C, rising by 0.1°C per 5 seconds, and analyzed by Precision Melt Analysis software (Bio-Rad Laboratories). The melt curve shape sensitivity and Tm difference threshold were set at 70% and 0.1°C, respectively, to distinguish wild-type from mutant alleles.[31]

Sanger Sequencing

The amplified products in the well that showed positive HRM analysis results were purified with the QIAquick PCR Purification Kit (Qiagen) and sequenced using the Bigdye Terminator v3.1 Cycle Sequencing Kit (Applied Biosystems, Foster City, Calif) with a 3130 DNA Analyzer (Applied Biosystems). The sequencing primers are listed in Supplemental Table 1, http://links.lww.com/MPA/A341. Conventional PCR was also performed on 10 specimens that were insufficiently amplified for HRM analysis, and they were subjected to Sanger sequencing (Fig. 1).

Competitive Allele-Specific TaqMan PCR

Competitive allele-specific TaqMan PCR (castPCR) using GNAS_27887_mu and GNAS_27895_mu probes (Applied Biosystems) was performed to detect R201C and R201H mutations. Mastermixes with 20 ng of genomic DNA were prepared as recommended by the manufacturer's protocol and distributed in a 96-well plate. The PCR conditions were 95°C for 10 minutes, followed by 5 cycles at 92°C for 15 seconds and at 58°C for 1 minute, and 40 cycles at 92°C for 15 seconds and 60°C for 1 minute. Real-time data were collected during the last 40 cycles of amplification and analyzed using Mutation Detector software v. 2.0 (Life Technologies, Carlsbad, Calif). Specimens with a delta Ct of less than 9.96 were considered positive for mutation, where dCt = Ct mut − Ct ref.[30]

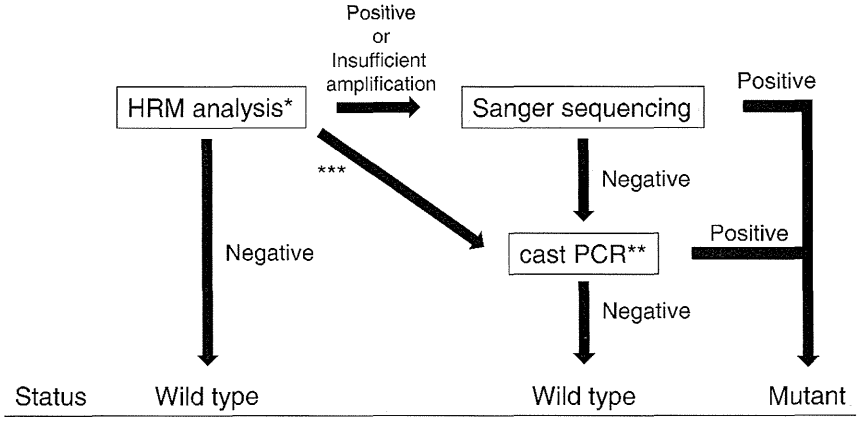

FIGURE 1. Schematic of methodology for the detection of *GNAS* mutation in tissue specimens. First, HRM* analysis was performed to evaluate *GNAS* mutation status in genomic DNA extracted from tissue specimens. The PCR products showing positive HRM analysis results were subjected to the Sanger sequencing. Specimens indicated to have a negative result by Sanger sequencing were tested by competitive allele-specific TaqMan PCR (castPCR**). ***Tissue specimens of IPMNs with distinct PDAC that showed negative HRM analysis results were subjected to castPCR to confirm the absence of *GNAS* mutation.

KRAS Mutation Detection

The mutation status of *KRAS* codon 12 and 13 was also assessed by HRM analysis and subsequent Sanger sequencing. The primers and annealing temperatures for HRM analysis and Sanger sequencing are listed in Supplemental Table 1, http://links.lww.com/MPA/A341.

Statistical Analysis

Statistical analysis was performed with JMP Pro 9.0.2 (SAS Institute Inc, Cary, NC). Continuous data are expressed as median and range. Comparison between 2 groups was performed using the Mann-Whitney *U* test for continuous data and the Fisher exact test for categorical data. The survival function was calculated by the Kaplan-Meier method. Differences in survival time were evaluated with a log-rank test. A 2-tailed *P* value of less than 0.05 was considered statistically significant. To detect the independent predictors of the presence of distinct PDAC in patients with IPMN, a multivariate logistic regression model was constructed. The variables with *P* values of less than 0.2 by univariate analyses were included in this model.

RESULTS

Comparative Analyses of Clinicopathologic Features and *GNAS* Status Between IPMN With and Without Distinct PDAC

The median age of this study cohort at the time of the initial operation was 70 years (range, 38–85 years), and there were 75 male (67%) and 37 female (33%) patients. The median surveillance period was 44 months (range, 7–188 months). Of 94 patients with IPMN without distinct PDAC, 70 (74%) had noninvasive IPMNs and 24 had invasive IPMNs. Although 4 patients with IPMN were affected by recurrent invasive IPMN in their residual pancreas,[32] the other 90 had no findings of either progression of IPMN or development of distinct PDAC in the remnant pancreas during the surveillance period. Therefore, metachronous development of distinct PDAC was not observed in any of the 94 patients with IPMN without distinct PDAC after the initial operation during the surveillance period.

Of 16 patients with IPMN with distinct PDAC, 2 had multifocal IPMNs in the resected specimen; therefore, 18 IPMN lesions were available for analysis. Sixteen (89%) of these 18 lesions were BD-IPMN, and the remaining 2 (11%) exhibited dilation of the main pancreatic duct: 1 was categorized as main duct IPMN (MD-IPMN); and the other, as mixed-type IPMN.

The results of the comparative analysis of clinicopathologic features between 16 patients with IPMN with distinct PDAC (13 synchronous, 2 metachronous, and 1 both) and 94 patients with IPMN without PDAC are shown in Table 1. *GNAS* codon 201 mutation was observed in 61 (65%) of 94 IPMNs without PDAC: 39 (71%) of 55 gastric type IPMNs, 15 (75%) of 20 intestinal-type IPMNs, 6 (30%) of 20 pancreatobiliary-type IPMNs, and 0 of 2 oncocytic-type IPMNs. The rate of *GNAS* mutation in IPMN with distinct PDAC was 25% (4/16), which was significantly lower than that in IPMN without PDAC ($P = 0.005$). Of these 4 IPMNs with *GNAS* mutation in the concomitant PDAC group, 2 were gastric type IPMN and 2 were intestinal-type IPMN. Notably, a significant difference in the detection rate of *GNAS* mutations was also found when the analysis was focused on gastric type IPMN with (16%, 2/12) and without concomitant PDAC (71%, 39/55) ($P = 0.0003$).

According to the multivariate logistic regression model, the absence of *GNAS* mutation and gastric type IPMN reached statistical significance as independent predictors of the presence of distinct PDAC (Table 2).

GNAS/KRAS Mutation Status in PDAC With Concomitant IPMN

Resected PDAC specimens were available for mutational analyses of *GNAS/KRAS* in 13 of 16 patients with PDAC with concomitant IPMN, including 2 with noninvasive carcinoma. Examination of all of these 13 PDACs with concomitant IPMN displayed the wild-type at *GNAS* codon 201, even when sensitive mutation scanning was performed. Mutation of *KRAS* codon 12 was observed in 11 (84%) of 13 PDACs with concomitant IPMN, and as a result, the status of *KRAS* codon 12 or *GNAS* codon 201 in all 13 PDACs differed from that in coexisting IPMN.

Stratification According to the Presence or Absence of *GNAS* Mutations in IPMNs: Analyses of Tissue Specimens

To assess the clinical significance of *GNAS* mutations in patients with various types of IPMN, the study subjects were stratified according to the status of *GNAS* codon 201 (Table 3).

Sixty-five patients had IPMN with *GNAS* mutation, including 4 (5%) with distinct PDAC. On the other hand, of 45 patients with IPMN without *GNAS* mutation, 12 (27%) had distinct PDAC (4/65 vs 12/45, $P = 0.005$). *GNAS* mutation in tumor cells was detected in 7 (32%) of 22 pancreatobiliary-type IPMN specimens; the frequency was significantly lower than that of the other subtypes ($P = 0.0067$).

The association between the epithelial subtypes of 45 IPMNs without *GNAS* mutation and the presence of distinct PDAC concomitant with IPMN was shown in Table 4. Distinct PDAC was more frequently observed in gastric type IPMN without *GNAS* mutation than in other subtypes (10/23, 43%, vs 2/22, 9%; $P = 0.017$, Table 4).

Mutational Analysis of *GNAS* Codon 201 in DF and Matched Tissue Specimens

Duodenal fluid specimens and matched tissue specimens were available from 23 patients, including 19 patients having IPMN without PDAC and 4 having IPMN with distinct PDAC (Table 5). In tissue specimens, *GNAS* mutation was detected in 12 (63%) of 19 IPMNs without PDAC and 1 (25%) of 4 IPMNs with distinct PDAC. As a result, a total of 13 (56%) IPMNs harbored *GNAS* mutation among the study subjects whose DF was analyzed. By castPCR, *GNAS* R201C or R201H mutation was found in 11 (48%) of 23 DF samples (Fig. 2A), and these mutation

TABLE 2. Multivariate Analysis of Potential Predictors of the Presence of PDAC With Concomitant IPMN

Variables	Odds Ratio	95% CI	*P*
Image branch duct size	0.96	0.9–1.0	0.13
Histopathologic grade: invasive	0.2	0.0098–1.3	0.098
Epithelial subtype of IPMN: gastric	4.1	1–21	0.049
Mural nodule: absent	1.3	0.33–5.8	0.69
GNAS mutations: absent	9.5	2.5–48	0.0007

CI, confidence interval.

TABLE 3. Comparative Analysis of Characteristics of IPMN According to Presence or Absence of *GNAS* Codon 201 Mutation

Variables		*GNAS* Mutation Present (n = 65)	*GNAS* Mutation Absent (n = 45)	*P*
Age	Median (range), y	71 (52–85)	67 (38–85)	0.29
Sex	Male	51 (78)	23 (51)	0.0037
	Female	14 (22)	22 (49)	
Location of IPMN	Pancreatic head	38 (58)	28 (62)	0.83
	Other	27 (42)	17 (38)	
Type of invasive carcinoma	Absent	52 (80)	19 (42)	0.0001
	Invasive carcinoma derived from IPMN	10 (15)	14 (31)	0.062
	Distinct PDAC	4 (5)	12 (27)*	0.0047
Morphological type	MD-IPMN	2 (6)	4 (13)	0.5
	Mixed	7 (23)	4 (13)	
	BD-IPMN	22 (71)	23 (74)	
Image branch duct size	Median (range), mm	30 (7–80)	25 (7–62)	0.35
Mural nodule	Present	30 (46)	15 (33)	0.23
	Absent	35 (54)	30 (67)	
Histopathologic grade of IPMN	LGD	27 (42)	15 (33)	0.43
	IGD	14 (22)	7 (16)	0.47
	HGD	14 (22)	8 (18)	0.81
	Invasive	10 (15)	15 (33)	0.037
Epithelial subtype of IPMN	Gastric	41 (63)	23 (51)	0.24
	Intestinal	17 (26)	5 (11)	0.057
	Pancreatobiliary	7 (11)	15 (33)*	0.0067
	Oncocytic	0 (0)	2 (4)	0.17
KRAS mutation	Present	45 (69)	30 (67)	0.56
	Absent	13 (20)	7 (16)	
	Undetermined	7 (11)	8 (18)	

The number in parentheses indicates the percentage of the total number of patients in each group.
*Times after initial diagnosis of IPMN.

statuses of DF samples were consistent with those of matched tissue specimens (Figs. 2B–D). *GNAS* mutation could not be detected in DF specimens in 2 patients with *GNAS* mutation in resected tissue specimens; 1 had gastric type IPMN with LGD (*GNAS* R201H) and distinct PDAC (*GNAS* wild-type), and the other had gastric type IPMN with IGD (*GNAS* R201H). Therefore, the accuracy of DF DNA testing to predict the *GNAS* status of IPMN was 91% (21/23). In 13 patients without *GNAS* R201C or R201H mutation in DF, 11 had IPMN without *GNAS* mutation, including 3 patients with distinct PDAC (Figs. 3A–D).

No adverse events were identified during or after DF collection and pancreatic juice cytology in 19 of 23 patients, whereas 4 patients with mild hyperamylasemia after ERCP were quickly and successfully treated with conservative medication.

DISCUSSION

This study focused on the association between the *GNAS* mutation status and the clinicopathologic features of IPMN, including those with distinct PDAC. The rate of *GNAS* mutations in IPMN with distinct PDAC was significantly lower than that in IPMN without distinct PDAC, and all coexisting PDACs also exhibited the wild-type at *GNAS* codon 201. We then analyzed the mutant status of DF obtained from patients with IPMN and showed the potential usefulness of DF specimens to determine the mutant status of IPMN.

Most PDACs concomitant with IPMN found in the same pancreas were simultaneously diagnosed and resected together with IPMN; however, we also experienced patients who had metachronous development of distinct PDAC during surveillance or after resection of BD-IPMN. Therefore, close attention should always be paid to the possible occurrence of concomitant PDAC at the time of initial assessment of IPMN as well as during surveillance of IPMN after resection or observation without resection. According to the clinicopathologic and mutational analyses of resected specimens of IPMN, 2 independent predictors, namely, gastric type IPMN and the absence of *GNAS* mutation in IPMN, were detected. The incidence rates of distinct PDAC in the current study subjects with IPMN, gastric type IPMN, and *GNAS* wild-type IPMN were 14%, 18%, and 27%, respectively. When we focused on patients having *GNAS* wild-type IPMN, 43% of gastric type IPMNs had distinct PDAC. Therefore, the evaluation of *GNAS* status as well as the subtype of IPMN possibly

TABLE 4. The Epithelial Subtype of *GNAS* Wild-type IPMN Stratified by the Presence or Absence of Distinct PDAC

Epithelial Subtype of IPMN	IPMN With PDAC	IPMN Without PDAC	*P*
Gastric	10	13	0.017
Intestinal	0	5	0.3
Pancreatobiliary	2	13	0.28
Oncocytic	0	2	1

TABLE 5. Clinicopathologic Features and *GNAS* Mutation Status of DF and Matched Tissue Specimens in 23 Patients Who Underwent Prospective DF Collection

Patient No.	Age, y	Sex	Location of IPMN	Location of Distinct PDAC	Lesion Type	Morphological Type	Cyst Size, mm	Mural Nodule	Histopathologic Grade	Subtype of IPMN	*GNAS* Summary, IPMN	*GNAS* Summary, Distinct PDAC	*GNAS* Mutation in DF	Pancreatic Juice Cytology
S-10	64	M	Ph	—	IPMN	Mixed	65	Present	IGD	Gastric	R201H	—	R201H	Class II
S-12	70	M	Ph	—	IPMN	BD-IPMN	80	Absent	HGD	Pancreatobiliary	R201H	—	R201H	Class IIIa
S-13	79	M	Pt	—	IPMN	BD-IPMN	45	Absent	LGD	Gastric	R201H	—	R201H	Class I
S-14	71	M	Ph	—	IPMN	BD-IPMN	34	Absent	IGD	Gastric	R201H	—	R201H	Class IIIa
S-15	68	M	Ph	—	IPMN	Mixed	21	Present	LGD	Gastric	R201H	—	R201H	Class IIIa
S-17	52	M	Ph	—	IPMN	BD-IPMN	62	Present	IGD	Gastric	R201H	—	R201H	Class V
S-18	70	M	Pb	—	IPMN	BD-IPMN	28	Absent	LGD	Gastric	R201H	—	R201H	Class III
S-21	56	M	Ph	—	IPMN	BD-IPMN	30	Absent	IGD	Intestinal	R201C	—	R201C	Class IIIb
S-22	55	M	Pb	—	IPMN	MD-IPMN	—	Absent	LGD	Gastric	R201H	—	R201H	Class IIIa
S-24	68	M	Pb	—	IPMN	Mixed	10	Present	IGD	Gastric	R201C	—	R201C	Class IV
S-16	54	M	Ph	—	IPMN	Mixed	15	Present	IGD	Gastric	R201H	—	Wt	Class IIIb
S-09	79	F	Pb	—	IPMN	BD-IPMN	30	Absent	LGD	Gastric	Wt	—	Wt	Class II
S-11	51	M	Pb	—	IPMN	Mixed	13	Absent	HGD	Intestinal	Wt	—	Wt	Class II
S-19	72	F	Pb	—	IPMN	BD-IPMN	23	Absent	IGD	Pancreatobiliary	Wt	—	Wt	Class IIIa
S-23	73	M	Pb	—	IPMN	BD-IPMN	35	Absent	HGD	Pancreatobiliary	Wt	—	Wt	Class V
C-04	70	F	Ph	Pb	IPMN with PDAC	BD-IPMN	50	Absent	LGD	Gastric	Wt	Wt	Wt	Class II
C-05	72	F	Ph	Pt	IPMN with PDAC	Mixed	23	Present	Invasive	Gastric	Wt	Wt	Wt	Class V
C-10	78	F	Ph	Pb	IPMN with PDAC	Mixed	17	Present	LGD	Gastric	R201H	Wt	Wt	Class V
C-15	82	F	Pt	Pt	IPMN with PDAC	MD-IPMN	—	Absent	LGD	Gastric	Wt	Wt	Wt	Unsuccessful ERP
I-01	52	F	Pt	—	Invasive IPMN	BD-IPMN	36	Absent	HGD	Pancreatobiliary	Wt	—	Wt	Class II
I-03	69	M	Ph	—	Invasive IPMN	BD-IPMN	21	Absent	HGD	Gastric	R201H	—	R201H	Class V
I-08	75	F	Pt	—	Invasive IPMN	BD-IPMN	50	Absent	HGD	Gastric	Wt	—	Wt	Unsuccessful ERP
I-13	58	M	Ph	—	Invasive IPMN	BD-IPMN	29	Absent	HGD	Pancreatobiliary	Wt	—	Wt	Class V

F, female; M, male; Pb, pancreatic body; Ph, pancreatic head; Pt, pancreatic tail; Wt, wild-type.

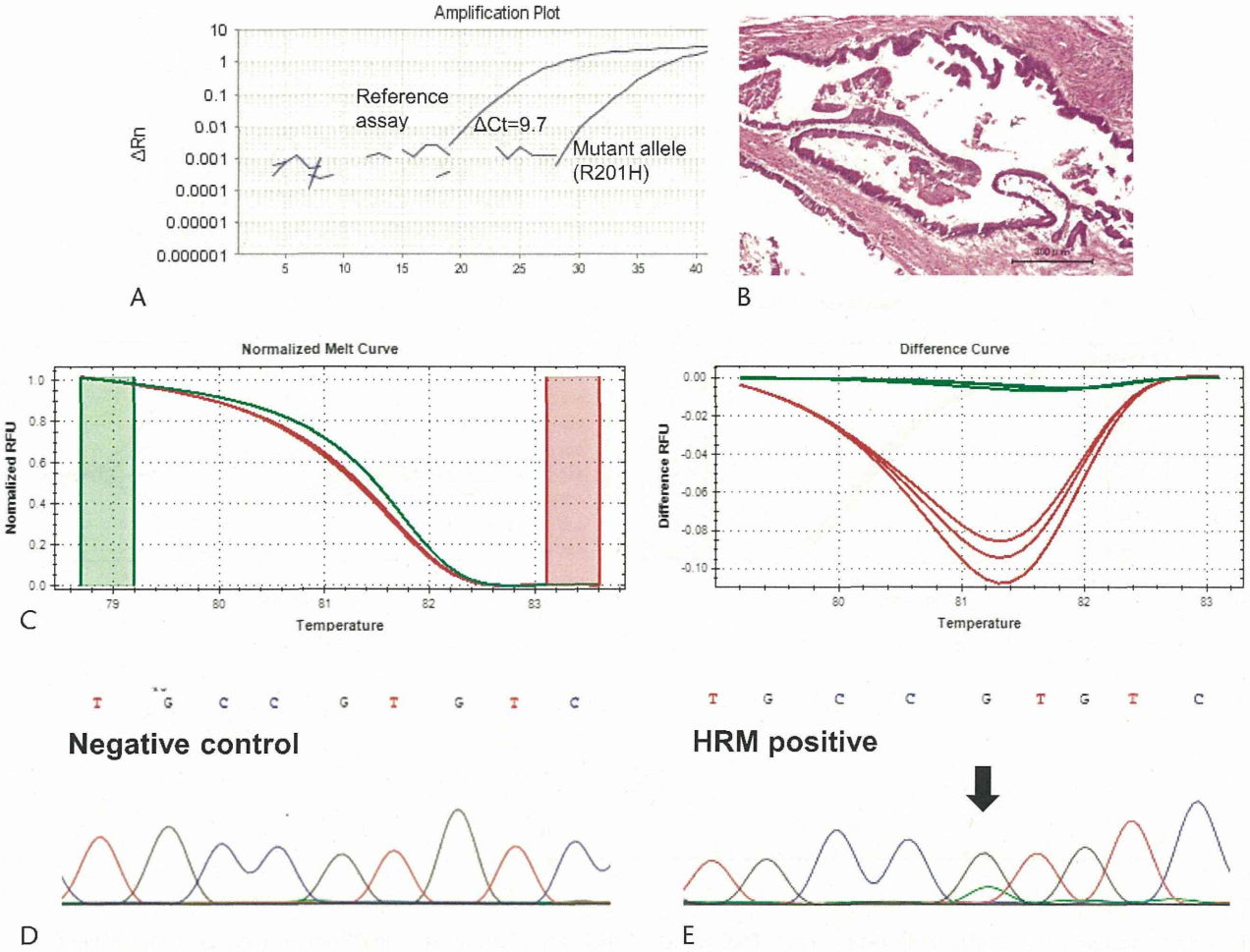

FIGURE 2. Representative case of IPMN of the pancreas exhibited *GNAS* codon 201 mutation in both preoperatively collected DF and resected specimens. *GNAS* R201H mutation was detected in DF obtained from a patient with IPMN by castPCR (A). Pathologic examination revealed gastric type IPMN with IGD (×100) (B). High-resolution melt curve analysis of tissue specimens indicated the presence of mutation in *GNAS* exon 8 (green lines: fluorescence of wild-type specimen, red lines: fluorescence of IPMN tissue specimen) (C), and subsequent Sanger sequencing confirmed *GNAS* R201H mutation (D: wild-type specimen, E: IPMN tissue specimen; arrow indicates mutation).

adds value in the surveillance of patients with IPMN in terms of the possible development of distinct PDAC. On the other hand, although preoperative subtyping of IPMN can often be accomplished using pancreatic juice cytology or cell block histology with mucin staining,[33,34] routine pancreatic juice cytology for benign-looking BD-IPMN is not recommended in the international consensus guidelines.[3] Therefore, we determined the *GNAS* mutation status using DF for patients with IPMN containing those with concomitant PDAC.

The frequency of *GNAS* mutation in resected IPMN seems to differ according to the method of detection of the genetic mutation. We screened the mutation status of *GNAS* exon 8 by HRM analysis and then confirmed the presence of *GNAS* point mutations at codon 201 by Sanger sequencing or castPCR. Of 110 surgically resected IPMN specimens, 65 (59%) harbored *GNAS* R201C or R201H mutations. In the Johns Hopkins study, the mutation status of 86 resected IPMN specimens was analyzed by ligation assays, BEAMing assays, or pyrosequencing, and 52 IPMN specimens (61%) harbored *GNAS* R201C or R201H mutations.[18,19] Therefore, the sensitivity of the methods used to detect *GNAS* mutation in this study seemed to be sufficient. Nevertheless, *GNAS* mutation was rarely found in IPMN with distinct PDAC, whereas most IPMNs and coexisting PDACs harbored *KRAS* mutations.

The situation of concomitant PDAC and IPMN reported in this study is similar to that in ordinary PDAC and pancreatic intraepithelial neoplasia (PanIN), most cases of which demonstrated mutated *KRAS* but wild-type *GNAS*.[35] Among the 4 epithelial subtypes of IPMN, gastric type IPMN has been regarded as a mimicker of PanIN because it is usually located in peripheral sites and shares many histologic and cytologic features with PanIN.[36] In addition, synchronous development of IPMN-like lesions, PanIN, and PDAC in the same pancreas was occasionally observed in a genetically engineered *KRAS*-mutated mouse model.[37] In this study, we found that the status of *KRAS* codon 12 and *GNAS* codon 201 in all examined PDACs differed from that in coexisting IPMN. These results indicate that IPMN and concomitant PDAC are not derived from the same precursor. Although it might be very difficult to explain why the occurrence of concomitant PDAC can be predicted by the presence of IPMN originated from a different precursor lesion, Johns Hopkins studies previously reported the similar findings that different *KRAS* gene mutations